

NASA Technical Paper 1300

**CASE FILE  
COPY**

# An Integrated Computer Procedure for Sizing Composite Airframe Structures

Jaroslav Sobieszczanski-Sobieski

FEBRUARY 1979

**NASA**

NASA Technical Paper 1300

An Integrated Computer  
Procedure for Sizing  
Composite Airframe Structures

Jaroslav Sobieszczanski-Sobieski  
*Langley Research Center*  
*Hampton, Virginia*



National Aeronautics  
and Space Administration

**Scientific and Technical  
Information Office**

1979

## CONTENTS

SUMMARY . . . . .	1
INTRODUCTION . . . . .	1
SYMBOLS . . . . .	2
OVERALL DESIGN APPROACH . . . . .	3
OPTIMIZATION PROCEDURE FOR SANDWICH PANELS . . . . .	5
Evaluation of Constraints . . . . .	5
Side constraints . . . . .	5
Stress constraints . . . . .	6
Buckling constraints . . . . .	7
Objective Function . . . . .	9
Optimization Algorithm . . . . .	9
VEHICLE MODEL . . . . .	9
Finite-Element Model . . . . .	9
Loading Cases . . . . .	10
Types of Construction . . . . .	10
Material . . . . .	10
Design Variables and Fixed Parameters . . . . .	11
RESULTS . . . . .	11
Comparison of Construction Type and Material . . . . .	11
Thickness distribution . . . . .	12
Criticality of buckling constraints . . . . .	12
Structural mass and stiffness characteristics . . . . .	13
Selection of Design Variables . . . . .	13
Distributions of thicknesses and orientation angles . . . . .	14
Influence on buckling behavior . . . . .	14
Changes in mass and stiffness characteristics . . . . .	14
Variables Constant Over Large Areas of Wing Cover . . . . .	15
Summary of Trends . . . . .	16
Convergence and Computational Requirements . . . . .	16
CONCLUDING REMARKS . . . . .	17
REFERENCES . . . . .	19
TABLES . . . . .	21
FIGURES . . . . .	26

Preceding Page Blank

## SUMMARY

A computerized algorithm to generate cross-sectional dimensions and fiber orientations for composite airframe structures is described, and its application in a wing structural synthesis is established. The algorithm unifies computations of aeroelastic loads, stresses, and deflections, as well as optimal structural sizing and fiber orientations in an open-ended system of integrated computer programs. A finite-element analysis and a mathematical-optimization technique are the main components of the procedure. Design constraints include stress, strain, local buckling, and minimum gage. The algorithm is applied to evaluate a series of basic design alternatives such as types of construction, types of material, and manufacturing restrictions for the low-aspect-ratio wing of a large transport airplane. Included also is a review of the computational efficiency of the method.

## INTRODUCTION

Extensive use of computer-aided design in synthesis of airframes for a low-aspect-ratio supersonic cruise airplane is reported in references 1, 2, and 3. The studies in reference 1 focused on the arrow-wing configuration. The objective was to size the wing structure for minimum mass, subject to static strength requirements. The basic wing was assumed to be constructed of ribs, spars, and sandwich cover panels. The variants considered in the sizing studies were an all-metal (titanium) wing, a wing of hybrid construction in which the cover panels were made of a graphite-polyimide composite, and, finally, an all-composite wing.

Because the airplane (ref. 1) was large and very flexible, it was important to include the effect of structural deformations on aeroelastic loads. This situation required detailed aerodynamic and structural analyses which were computationally very large. In some of the studies presented in reference 1, composite materials were assumed to be used for wing construction. Composite materials allow the designer the added flexibility of adjusting the proportions of material at the various orientations and the orientation angles themselves. This added design flexibility increases the number of design variables and further adds to the complexity of the sizing problem.

As indicated in reference 4, most available procedures for optimizing composite structures are for isolated components of large structures. (See refs. 5 to 7.) In addition, there is a continuing effort for improvement in the efficiency of optimization procedures to extend their applicability to entire structures. (See refs. 8 to 13.) Because of computational size and need to optimize at the detail design level, the subject problem entails characteristics of the synthesis on both component and large structure levels.

The purpose of this paper is to document the procedure used in the studies of reference 1, to explain the algorithm details, and to give a more detailed account of several structural sizing trade-offs.

Nick J. Santoro, Southern Company Services, Inc., Birmingham, Alabama, participated in the conceptual part of the reported work while with Vought Corporation, Hampton Technical Center, Hampton, Virginia, and was responsible for generation of the numerical results.

#### SYMBOLS

Values are given in both SI and U.S. Customary Units. The calculations were made in U.S. Customary Units.

$A, B, D$	matrices of membrane stiffness, bending plate stiffness, and bending-membrane coupling stiffness, respectively
$a, b$	rectangular panel dimensions (see fig. 2)
$g_i$	dimensionless measure of constraint satisfaction
$I$	set of constraints
$k$	vector of plate curvatures due to bending
$M$	vector of moments
$m$	mass of core face-sheet bonding material per unit area
$m_{dep}, m_{indep}$	nonoptimum structural mass dependent on panel area and independent of panel area, respectively
$m_p$	structural mass of panel defined by equation (10)
$N$	vector of membrane force
$N_x, N_y, N_{xy}$	normal and shear membrane forces acting on edges of panel (see fig. 2)
$S$	panel area
$t$	thickness of material whose fibers are oriented at a given angle
$t_c$	"caliper" thickness of sandwich panel (face-to-face)
$t_t$	sum of thicknesses of both face sheets
$t_\phi, t_\gamma$	thickness of material whose fibers are oriented at $\phi$ and $\gamma$ , respectively
$t_{i,n}$	thickness of $i$ th ply and total number of plies in one face sheet of symmetric sandwich
$y$	behavior variable

$\gamma_a$  limit on behavior variable (allowable value)  
 $Z$  defined by equation (6)  
 $\epsilon$  vector of membrane strains  $\epsilon_x, \epsilon_y, \epsilon_{xy}$  or  $\epsilon_1, \epsilon_2, \epsilon_{12}$   
 $\rho$  mass density of ply material  
 $\rho_c$  mass density of core  
 $\sigma_1$  stress in fiber  
 $\sigma_2$  stress in matrix, normal to  $\sigma_1$ , in ply plane  
 $\sigma_{1t}$  allowable tension limit of fiber  
 $\sigma_{2t}, \sigma_{2c}$  allowable tension and compression matrix limits  
 $\tau_{12}$  in-plane shear stress  
 $\phi, \gamma$  orientation angles of fibers (see fig. 2)

Subscripts:

$a$  allowable limit  
 $cr$  critical

Configurations:

$B$  metal baseline construction  
 $LM/H$  low Young's modulus/hybrid construction  
 $HM/H$  high Young's modulus/hybrid construction  
 $LM/P$  low Young's modulus/pure composite construction  
 $HM/P$  high Young's modulus/pure composite construction  
 $LM/H-CA$  conservative allowable strain variant of LM/H configuration

OVERALL DESIGN APPROACH

Airplane flexibility introduces a coupling of aerodynamic loads and structural displacements. This coupling can be accounted for by organizing the analyses involved into an iterative process. The flow chart in figure 1 (from ref. 14) depicts a particular organization of the iterative process used in this study.

Two iterative loops are shown in the flow chart of figure 1. Loop I begins with the computation of aerodynamic loads on the entire airplane whose shape is preset to the defined cruise shape (best for cruise aerodynamic efficiency). Initially, the same shape is used to compute loads for both cruise and maneuver. The loads are subsequently applied to the airframe using the initial cross-sectional dimensions, and the ensuing analysis yields displacement and stresses for both cruise and maneuver. The cruise displacement outputs are used to calculate the jig shape (shape to which the airframe is to be built to attain the desired shape under cruise loads). The jig shape and the maneuver deflections are superimposed to calculate maneuver shape. The loop is closed by feeding back the maneuver shape to calculate a new set of aerodynamic loads for maneuver.

In the flow chart of figure 1, loop II involves use of the stress outputs to resize the airframe structural components. Resizing of structural components produces new cross-sectional dimensions (e.g., wing-cover thicknesses) which are fed back to the structural analysis input. Following the method established in reference 14, the iteration process alternates between loops I and II. The flexibility of the system allows the user to choose the execution sequencing that best fits the problem at hand. A typical mix of the loops is three executions of loop I for each execution of loop II. Details of the system organization are described in reference 15, and an outline of the major analysis programs involved is provided in reference 16. All data transfers shown by the flow chart in figure 1 are fully computerized. The iterative process continues until the convergence criteria for aerodynamic loads, structural mass, and stresses are satisfied.

Structural resizing is executed for each structural component separately as if that component, together with the forces acting on it from the neighboring components, were extracted from the surrounding structure. In this way, an independent problem of structural optimization is formulated with respect to the component forces which are treated as invariant external loads. Mathematical nonlinear programming is used to solve this problem for each structural component. After all components have been optimized, new aeroelastic loads are computed, the total structure is reanalyzed, and new component forces are generated for use in the next round of individual component optimizations.

As pointed out in reference 17, where this approach and its positive and negative implications are discussed in detail, the disadvantage of such a decomposition of the problem is that optimization of components is not tantamount to optimization of the whole; or, in other words, minimization of the individual component masses does not guarantee minimization of the total mass. This situation is caused by the inability to control the load path on the assembled structure level; in this regard, the procedure resembles the fully stressed design (FSD) algorithm. The advantages lie in the drastically reduced dimensionality of each of the individual optimization problems that must be solved and in the inherent modularity of the solution algorithm. The consequence of the former is that the required computer resources stay within reasonable bounds. The modularity permits selection of the resizing algorithm considering generality, efficiency, and accuracy in isolation from the rest of the problem. Details of the component optimization procedure are described in the following section.

## OPTIMIZATION PROCEDURE FOR SANDWICH PANELS

The object of the optimization procedure for each individual panel is to minimize the panel mass subject to constraints of stress, strain, panel buckling, and minimum gage. Panel load consists of the membrane forces  $N_x$ ,  $N_y$ , and  $N_{xy}$  shown in figure 2. These forces are held constant for the duration of each consecutive optimization procedure for individual panels. For metal panels, the design variables are the face-sheet thickness and the total sandwich thickness. For composite panels, the variables are the thickness of the composite material laid at a given orientation angle (layer thickness), the orientation angles themselves, and the total sandwich thickness. Construction of a composite sandwich panel and the design variables are shown in figure 2. Organization of the procedure is depicted in figure 3. The flow chart of figure 3 corresponds to the box marked "RESIZE ELEMENTS" in figure 1. A panel defined by the design variables and subject to the given loads is analyzed (box 1 in fig. 3) for strain, stress, and panel buckling. Output from the analysis is used to evaluate constraints and the objective function which is the mass of the panel. Subsequently, the results of this evaluation are used by a general purpose optimizer (box 2) to calculate a new set of design variables modified to reduce the objective function and to move toward satisfaction of the panel constraints. Operations 1 and 2 are repeated until the constrained minimum mass is reached. Then, the procedure is repeated for each next consecutive panel until all panels have been optimized. When all panels have new dimensions, the wing structure is reanalyzed for aerodynamic loads and internal forces (loops I and II in fig. 1) and another round of the individual panel optimization procedure is carried out.

### Evaluation of Constraints

The optimization algorithm requires that the degree of violation or satisfaction of the constraints be stated in the following standard, dimensionless form:

$$g_i(y, y_a) \leq 0 \quad (i \in I) \quad (1)$$

where  $g_i = \frac{y}{y_a} - 1$  symbolizes the  $i$ th constraint,  $y$  is a behavior variable

such as stress, etc., and  $y_a$  is the corresponding allowable value of  $y$  dictated by the material limits (yield stress, ultimate stress, etc.) or resulting from the structural stability considerations, i.e., computation of the critical buckling stresses. The purpose of the analysis of the panel being optimized is to supply values of  $y$  and  $y_a$  used in equation (1).

Side constraints.— The side constraint (minimum gage) values for the skins are set to provide, as a minimum, four plies in each face sheet of the sandwich. These plies are associated in pairs with orientation angles  $\phi$  and  $-\phi$ . In



most cases  $\phi$  is selected to be  $45^\circ$ . Thicknesses associated with other orientations, that is  $0^\circ$  and  $90^\circ$ , are permitted to vanish but not to become negative; therefore, their minimum gage is zero.

Upper limit on the skin thicknesses is provided indirectly by imposing a minimum gage value on the sandwich core thickness as a fraction of total sandwich thickness. Without such constraint, the face thicknesses could grow inward to the extent of eliminating the core.

Stress constraints.- Standard, anisotropic membrane analysis (ref. 18) is used to produce the stress-strain output for each ply for given edge forces and plate geometry. The analysis is simplified by the following assumptions:

(1) The face-sheet plies are symmetric with respect to the midsurface of the sandwich panel.

(2) The material associated with each orientation is uniformly dispersed throughout each face of the sandwich.

(3) The lay-up is orthotropic ( $t_\phi = t_{-\phi}$ ) although the axes of orthotropy need not be aligned with the panel sides (general orthotropy). As shown in figure 2, the orthotropy axes are oriented at an angle  $\gamma$  with respect to the x-axis coinciding with the panel side.

The result of assumption 1 is a decoupling of the basic force-deformation equation, from reference 18,

$$\begin{bmatrix} N \\ - \\ M \end{bmatrix} = \begin{bmatrix} A & B \\ - & D \end{bmatrix} \begin{bmatrix} \epsilon \\ \\ k \end{bmatrix} \quad (2)$$

into the equations  $N = A\epsilon$  and  $M = Dk$ . Assumption 2 permits evaluation of the terms of matrices A and D independent of the stacking sequence, and assumption 3 simplifies the buckling analysis.

Solution of the membrane problem represented by  $N = A\epsilon$  yields, for each fiber orientation, stresses parallel and perpendicular to the fibers  $\sigma_1$  and  $\sigma_2$ , the in-plane shear stress  $\tau_{12}$ , and the corresponding strains  $\epsilon_1$ ,  $\epsilon_2$ , and  $\epsilon_{12}$ . These values are combined with the allowable limits in constraint equations in the standard form shown in equation (1). For example, if  $\sigma_1 \geq 0$ ,

$$\frac{\sigma_1}{C_t \sigma_{1t}} - 1 = 0 \quad (3)$$

where  $\sigma_{1t}$  is an allowable tension and  $C_t$  is an associated factor used to modify the allowable stress for selected load cases. A typical example is the reduction of the allowable stress level for a 1g cruise condition due to fatigue considerations. All numerical information on load factors and allowable stress reduction factors actually used in this study is reported in the section on the vehicle model.

In order to prevent matrix failure, the strength constraints are of the form given in reference 19:

$$\left(\frac{\sigma_1}{\sigma_{1a}}\right)^2 - \left(\frac{\sigma_1\sigma_2}{\sigma_{1a}}\right)^2 + \left(\frac{\sigma_2}{\sigma_{2a}}\right)^2 + \left[\frac{\tau_{12}}{(\tau_{12})_a}\right]^2 - 1 \leq 0 \quad (4)$$

where  $\sigma_{2a} = \sigma_{2t}$  if  $\sigma_2 \geq 0$ , or  $\sigma_{2a} = \sigma_{2c}$  if  $\sigma_2 < 0$ . This constraint (eq. (4)) is a dimensionless inequality equivalent to the standard form represented by equation (1). All stress constraints are evaluated for each fiber orientation and for each loading case. In addition to these constraints, strain components of a sandwich panel are kept from exceeding specified limits by setting the following constraints:

$$\frac{|\epsilon_x|}{|\epsilon_{x,a}|} - 1 \leq 0 \quad (5)$$

where the subscript x (or y) refers to the panel coordinate that has at least one axis aligned with one of the panel sides and the subscript a denotes corresponding allowable strains. These overall constraints are useful since they provide a degree of additional control over the panel strain levels. This control is important for at least two reasons: (1) To meet the structure's overall stiffness requirements, i.e., those dictated by anticipated aeroelastic problems while still at the strength design stage and (2) To protect the panel edge members from overstress which may occur, for example, in the case of titanium spar caps framing a composite panel. (See section "Types of Construction.")

Buckling constraints.- Buckling of a plate such as the one shown in figure 2 cannot be solved exactly in a closed analytical form because of the general orthotropy and arbitrary in-plane loads. Since numerical buckling analysis is too costly in the repetitive application required in optimization, an approximate but fast method is used involving analytical solutions given in reference 20 for plates of special orthotropy. The special orthotropy assumption results in neglecting the bending-twist coupling terms  $D_{16}$  and  $D_{26}$  and appears to be justified for this type of application by the findings of reference 21.

According to reference 20, the general state of load is separated into the cases of biaxial normal stress and shear stress. The measure of buckling criticality due to biaxial membrane forces is given by the quantity

$$Z = \frac{\left[ N_x \left( \frac{m}{a} \right)^2 + N_y \left( \frac{n}{b} \right)^2 \right]}{\pi^2} \bigg/ \left[ D_{11} \left( \frac{m}{a} \right)^4 + 2D_{12} \left( \frac{mn}{ab} \right)^2 + D_{22} \left( \frac{n}{b} \right)^2 \right] \quad (6)$$

where  $m$  and  $n$  are the number of half-waves of the buckling deformation functions in the  $x$ - and  $y$ -directions, respectively.

The plate buckles when  $Z \geq 1$ , for any combination of  $m$  and  $n$ . The combination that minimizes  $Z$  is searched for numerically. A conservative approximation to the critical shear is obtained by the formula (ref. 20), for an infinite length strip,

$$(N_{xy})_{cr} = 4c \frac{[D_{11}(D_{22})^3]^{1/4}}{b^2} \quad (7)$$

where  $c$  is given numerically in reference 20 as a function of the parameter  $\frac{(D_{11}D_{22})^{1/2}}{D_{33}}$ . The combined action of the biaxial normal forces and the shear is described by the interaction equation, which forms the buckling constraint,

$$Z + \frac{\left[ \frac{N_{xy}}{(N_{xy})_{cr}} \right]^2}{-1} \geq 0 \quad (8)$$

Satisfaction of equation (8) guarantees satisfaction of the following special cases:

$$Z - 1 \leq 0 \quad (N_{xy} = 0) \quad (9a)$$

and

$$\frac{\left[ \frac{N_{xy}}{(N_{xy})_{cr}} \right]^2}{-1} \leq 0 \quad (N_x = N_y = 0) \quad (9b)$$

## Objective Function

The structural mass of the panel  $m_p$  is the objective function. The variable part of that mass is the sum of face-sheet mass and core mass and is a function of the thickness variables. In addition, a constant part is also included to represent masses of the bonding and of the nonstructural material ( $m_{dep}$  and  $m_{indep}$ ) according to the formula

$$m_p = 2 \sum_{i=1}^n [\rho t_i S + \rho_c S (t_c - t_t) + mS + m_{dep}S + m_{indep}] \quad (10)$$

## Optimization Algorithm

The optimization algorithm, represented by box 2 in figure 3, used for the optimization of composite panels is a method of feasible-usable directions, originally due to Zoutendijk (ref. 22), coded in a program described in reference 23. This algorithm turned out to be efficient, converging relatively independent of the number of design variables for the reported application.

## VEHICLE MODEL

The structural sizing algorithm described in the foregoing section is applied to the structural box of the low-aspect-ratio arrow wing of a supersonic-transport configuration. The basic details of the finite-element model of that configuration, as well as loads, materials, and design variables, are given in the following section.

### Finite-Element Model

The finite-element model is shown in figure 4. It is symmetric with respect to the airplane longitudinal center line with one-half consisting of 746 grid points and 2141 degrees of freedom connected by 2369 structural finite elements. The model represents wing, fuselage, vertical and horizontal tails, wing fins, engines, and engine mounts. Nonstructural masses of the engines, leading- and trailing-edge devices, and fuel tanks with fuel are included. The wing is modeled as follows:

- (1) Spar and rib caps - rod elements having only extensional stiffness
- (2) Spar and rib webs - quadrilateral panels having only shear stiffness
- (3) Wing covers - quadrilateral and triangular membrane elements, isotropic for metal covers and anisotropic for composite covers
- (4) Engine mounts - bar elements having extensional, bending, and torsional stiffnesses

- (5) Wing fins and tail - quadrilateral or triangular plane elements having in-plane and bending stiffnesses
- (6) Fuselage frames - rod elements
- (7) Fuselage longerons - rod elements
- (8) Fuselage skin - quadrilateral or triangular membrane elements

Since the fuselage structure is not included in the resizing process, the finite-element model of the fuselage is less detailed than the wing. A box beam is used for the fuselage and is composed of quadrilateral membrane elements and shear panels preserving the mass distribution of the fuselage and its overall bending and torsional stiffnesses. Statistically derived distributed nonoptimum and nonstructural masses are accounted for by appropriate coefficients.

### Loading Cases

From the multitude of loading cases usually considered in airframe design, the three cases selected and consistently used in this study were: 2.5g maneuver at Mach 1.2, -2g taxi at Mach 2.7, and 1g cruise at Mach 2.7. These cases constitute a minimal set of loadings needed for comparisons of the construction alternatives and for methodology evaluation. The rationale for their selection is as follows: (1) the maneuver loads generate the largest bending and shear forces near the wing root; (2) negative taxi loads activate buckling constraints in the bottom cover of the wing; and (3) constraining the level of stress due to the cruise loads is a simplified way to control airframe fatigue life. Because of aircraft flexibility and difference in Mach numbers, the maneuver and cruise load distributions differ significantly from each other. Therefore, stresses corresponding to one of these two load cases cannot be obtained by scaling stresses caused by the other.

### Types of Construction

In this study, a structure made entirely of titanium is adopted as a baseline design against which the composite construction results are compared. Two types of composite construction are considered for the wing: (1) a mixed, or hybrid, type in which only the sandwich-panel face sheets are replaced with composite material while the remainder of the structure is made of metal and (2) a pure composite construction in which all parts, except the aluminum honeycomb sandwich core, are made of composite material.

### Material

The titanium data used are displayed in table I. The allowable stress level for cruise is restricted to the value of  $F_{ac}$  to approximately account for fatigue requirements. In titanium construction, this value corresponds to a notch factor of 4.0. The data for the honeycomb core and core face-sheet

bonding are also included in table I. The composite material used in hybrid and pure composite construction is graphite-polyimide.

Graphite-polyimide is a composite material of interest for supersonic-cruise applications because of its relatively good retention of mechanical properties at elevated temperatures. The material properties anticipated for 1986 (ref. 2) are displayed in table I. In addition, a reduced allowable strain is considered to establish a safe bound on the fiber stress allowables. The fiber volume is assumed to be 60 percent throughout. The composite is assumed available in a low Young's modulus, high-strength version and in a high Young's modulus, low-strength version. In the discussion to follow, use of the low-modulus version is assumed unless otherwise indicated. Insofar as the fatigue stress allowable for cruise is concerned, no data similar to those used for titanium construction exist for composites. However, for consistency, the same ratio of the allowable cruise stress to the design limit stress is used for composites and for titanium.

### Design Variables and Fixed Parameters

In the design studies reported in the next section, wing area, planform, airplane mass, and structural layout are kept constant. Subject to change are the type of construction and the material. Within each of these discrete choices, the continuous variables for hybrid and pure composite constructions are selected from the set and include sandwich depth ("caliper" thickness)  $t_c$ ; thicknesses of the layers  $t_0$ ,  $t_\phi$ , and  $t_{90}$  associated with orientation angles  $0^\circ$ ,  $\pm\phi$ , and  $90^\circ$ , respectively; and the orientation angles  $\gamma$  and  $\phi$ . (See fig. 2.) Thus, the largest number of variables is six since the balanced laminate assumption of  $t_\phi = t_{-\phi}$  holds. In order to address the obvious manufacturing requirements, grouping of some of these design variables over blocks of adjacent panels is also considered. For the case of metal construction (baseline), the variables are sandwich thickness  $t_c$  and face thickness  $t_t$ .

## RESULTS

Numerical results obtained for the arrow-wing structure are presented in this section. The results pertain to three major consecutive phases of the study: (1) comparison of construction type and material, (2) optimization with the design variables determined most effective, (3) reoptimization with reduced number of design variables (grouping) to assess penalty for uniformity required for manufacturing. Results discussed in this report represent a strength design in which no attempt is made to control the wing stiffness and flutter.

### Comparison of Construction Type and Material

Several alternative designs are compared in terms of total sandwich-cover structural masses, distributions of the sandwich-cover face-sheet thickness over the wing, criticality of the buckling constraints, and stiffness characteristics.

Thickness distribution.- The distribution of total thickness  $t_t$  is shown for the titanium baseline configuration in figure 5(a) and for the composite configurations in figures 5(b), (c), (d), and (e). The corresponding masses are recorded in table II. The masses represent the total of two wings, including nonoptimum mass.

In this phase of the study, the design variables are face-sheet thickness for the titanium baseline configuration and thicknesses associated with  $0^\circ$ ,  $\pm 45^\circ$ , and  $90^\circ$  angles of fiber orientation for the composite configurations, with sandwich depth fixed at  $t_c = 1$  in. for all configurations. A high Young's modulus, low-strength version of the composite material is used. As seen in figure 5(a), the distribution is characterized by the thickness plateaus A and B, which correspond to the location of the wing fin and engine mount, respectively. A similar thickness distribution for the hybrid construction can be seen in figure 5(b). Maximum thicknesses for the hybrid construction (figs. 5(b) and (d)) are about twice the thickness for titanium construction. However, this is more than compensated for by the lower density of the composite material, which results in the mass savings discussed subsequently.

Eliminating the titanium caps and changing the shear web material from titanium to  $\pm 45^\circ$  composite turns the structure into a pure composite construction with the skin thickness distribution shown in figure 5(c). With titanium caps removed, the composite must carry a greater load; therefore, thickness builds up (as seen in fig. 5(c)) to values higher by about 25 to 50 percent, compared with the hybrid construction.

Thickness contours of the individual plies of  $90^\circ$  and  $\pm 45^\circ$  orientation angles are shown in figure 5(e) for the LM/H configuration. The contours (fig. 5(e)) indicate a characteristic concentration of the  $\pm 45^\circ$  orientation material in the area where the load path curves toward the wing root from the direction established by the wing sweep angle. Concentrations typical for total skin thickness are reflected in the distribution of the  $90^\circ$  orientation (spanwise) material.

In some instances these concentrations illustrate a well-known instability potentially inherent in a fully stressed design approach. Under that approach, an overstressed element is stiffened, thus attracting more load which in turn requires more stiffness in the next resizing cycle. An example of such thickness buildup is designated "region C" in figure 5(d). This numerical instability can be checked by imposing upper-limit side constraints on the thickness variables in the optimizer.

Criticality of buckling constraints.- The panels which evolve from the optimization as being critical in buckling are shown in figures 6(a) and (b). Comparison with figure 5(d) indicates correspondence of the thickness ridge and row A of buckling critical panels in figure 6(a). Removal of the titanium spar caps puts all the load on the composite panels, thus increasing very significantly the buckling critical area of a low Young's modulus wing cover. (See fig. 6(b).) The change to high Young's modulus material is effective in reducing the number of buckling critical panels to just two panels in figure 6(a) and one panel in figure 6(b).

Structural mass and stiffness characteristics.- Attention is now turned to such overall structural characteristics as structural mass and stiffness. Total structural mass of two wings includes mass of face sheets, core, bonding, ribs, and spars. Both webs and caps are accounted for in the latter, except for a pure composite construction in which there are no structural caps. Appropriate nonoptimum mass is added to all structural components. Static stiffness can be characterized by wing tip deflection (relative to the wing root) under 2.5g pull-up maneuver load, and stiffness can be partially measured by the natural frequency of the wing first bending mode.

The three wing characteristics, mass, tip deflection, and fundamental frequency, are represented by a vertical bar diagram in figure 7 for the B, LM/H, HM/H, LM/P, HM/P, and LM/H-CA configurations. Comparison of the bars shows a significant, 20-percent decrease in structural mass brought about by changing from the B configuration to the LM/H configuration. That benefit is partly offset by an increase in the wing tip deflection and a loss in the frequency of the wing first bending mode.

The loss of stiffness is caused by the fact that the ratio of the allowable stress of the composite to that of titanium is higher than the ratio of the respective Young's moduli, and is also strongly influenced by changes in thicknesses associated with different orientation angles. Lower strength but higher Young's modulus of the HM/H configuration reduces the mass by 13 percent and increases stiffness, as manifested by a drop in the wing tip deflection.

A drastic mass reduction of 56 percent is observed in the LM/P configuration, but it is countered by an equally sharp increase of the wing tip deflection. However, there is a small decrease of frequency because of the attendant decrease in mass. These effects are caused by the removal of the titanium caps with their contribution to the mass and their limiting influence on the composite strains. (See previous discussion on the constraints protecting the titanium caps from overstress in a hybrid construction.)

The HM/P configuration diminishes the mass savings to 49 percent but radically improves stiffness, as indicated by significant reduction of the wing tip deflection and rise in the wing frequency, the latter being tempered somewhat by growth of the structural mass. The influence of the imposition of a conservative strain allowable in the LM/H variant (LM/H-CA configuration) is seen to cause the mass reduction to drop to 16 percent (from 21 percent noted previously). The wing tip deflection decreases slightly from the baseline, but the wing frequency increases because of reduction in mass.

In summary, data collected in figure 7 and table II show the maximum mass savings to be 56 percent of the baseline mass when the configuration used is the low Young's modulus pure composite construction (LM/P).

### Selection of Design Variables

The subset of design variables consisting of three thicknesses for orientation angles fixed at  $0^\circ$ ,  $\pm 45^\circ$ , and  $90^\circ$  has been used so far. Effects of freeing the other design variables are now assessed for the LM/H-CA configuration.



Distributions of thicknesses and orientation angles.- Distributions of the thicknesses are illustrated in figures 8(a) and (b), which show contours of total thickness of all layers in both faces of the upper wing cover sandwich panels. Figure 8(a) corresponds to the layer thicknesses  $t_0$ ,  $t_\phi$ ,  $t_{90}$ , sandwich depth  $t_c$ , and orientation angle  $\phi$ . All thicknesses  $t$  and  $t_c$  are free design variables while orientation angle  $\gamma$  is kept constant at a value of  $90^\circ$ . Figure 8(b) corresponds to the set of design variables reduced to  $t_0$ ,  $t_\phi$ ,  $t_{90}$ , and  $\gamma$  while freezing  $t_c$  and  $\phi$  ( $\phi = 45^\circ$ ); figure 8(c) illustrates the result of freezing the variable  $t_c$  and thicknesses  $t_0$ ,  $t_\phi$ , and  $t_{90}$  while freezing the angles  $\gamma$  and  $\phi$  at  $90^\circ$  and  $45^\circ$ , respectively; and finally, figure 8(d) depicts the result for all six design variables being simultaneously free. Comparison of the results in figure 8 shows significant changes of the cumulative ply thickness distribution caused primarily by the smoothing effect of the variable  $t_c$ . This effect is due to the fact that the sandwich depth increase is a very efficient means of alleviating the panel buckling.

Individual ply thicknesses and orientation angles  $\phi$  are presented in figure 9(a) for variable  $\phi$  and constant  $\gamma$ . Orientation angle is indicated in figure 9(a) by arrows for each panel (numerals at each arrow denote the associated ply thickness). The orientation-angle distribution reveals that diagonal fibers associated with angle  $\phi$  tend to align with the spanwise fibers in the rear of the inboard wing box, which is dominated by bending moment. A significant number of angles  $\phi$  close to conventional  $\pm 45^\circ$  orientation is found in the front upper portion of the inboard wing box, where the load path is turning toward the fuselage as it comes from the outboard wing.

Numerical values of angles  $\gamma$  and  $\phi$  when both are used as optimization variables are shown in figure 9(b). It is apparent that the original setting of  $\gamma = 0^\circ$  (or close to it) is preserved by the optimizer over a great portion of the wing area. The only wing areas where it is advantageous to alter  $\gamma$  in the optimization process are in the vicinity of the wheel well, over the outboard wing tip, and near the fin attachment, where the structural layout causes abrupt changes of the load path direction.

Influence on buckling behavior.- The location of the buckling critical panels over the wing depends significantly on the choice of design variables, as revealed by comparing the different combinations in figures 10(a), (b), (c), and (d) with figure 6(a). Adding more design variables permits satisfaction of the stress-strain constraints with less material and, therefore, makes buckling significantly more critical; this is illustrated by the greater number of buckling critical panels in figures 10(b) and (d) than in figure 6(a). Increase in the number of such panels over the lightly loaded front part of the inboard wing (fig. 10(c)) indicates that the sandwich depth  $t_c$  is decreased to reduce the core mass.

Changes in mass and stiffness characteristics.- Variations of the thickness distributions caused by different choices of design variables have a cumulative impact on total mass, as indicated by values collected in table III. The table is arranged to show progressively lower mass from top to bottom brought about by the design variable choices listed. This arrangement reveals a general trend of structural mass decrease brought about by greater design freedom, that is, a

larger number of design variables which are free to change under the control of the optimization algorithm. Thus, a change from "thickness only" to "all six" design variables reduces the mass of the sandwich covers (sum of column 3 and column 4) by 21.5 percent and the total mass by 9.4 percent. A comparison of mass differences points to the sandwich depth  $t_c$  as the most effective variable in reducing mass. Angle  $\phi$  consistently causes more change than angle  $\gamma$ , which is the least effective variable. The effect of  $\phi$  is somewhat magnified when coupled with  $t_c$ , as shown by comparison of relative mass decrements in the third and seventh rows of table III.

The wing-tip-deflection column of table III shows that activating the angle design variables reduces stiffness more than structural mass. The variable  $t_c$  has a similar effect, although it appears to be less detrimental to stiffness than the variables  $\phi$  and  $\gamma$ . The loss of stiffness which accompanies the mass reduction can be attributed to the lack of the stiffness constraints in the optimization.

Results presented in this section identify the sandwich depth  $t_c$  and orientation angle  $\phi$  as the design variables, besides the ply thicknesses, which appear to be most effective under the particular set of loads and constraints. However, there are obvious manufacturing constraints that limit the design variable freedom. It lies within the procedure capability to address, at least partially, some of these constraints, as described in the following section.

#### Variables Constant Over Large Areas of Wing Cover

In the foregoing discussion, the manufacturing constraints are set aside, temporarily, in order to permit an unrestricted exploration of the benefits that may be brought about by freeing those design variables, such as orientation angles, which under a conventional approach would probably remain fixed.

Among the design variable choices considered, the proposition of varying orientation angles  $\phi$  and  $\gamma$  for each panel separately is the least producible one. However, inspection of the  $\phi$  and  $\gamma$  distributions over the wing, such as shown in figure 9(b), suggests the possibility of grouping.

Examples of grouping for variables  $\gamma$  and  $\phi$  are illustrated by figures 11(a) and 11(b), respectively. Similarly, grouping of sandwich depth  $t_c$  is depicted in figure 11(c). The effect is that rather large wing areas, e.g., almost the whole "glove" region, may be assigned a single value of a particular variable. The question of whether or not the groupings shown go far enough to render the extra manufacturing cost justifiable can only be answered on a case-by-case basis; the point to be made here is simply that such a grouping can be made.

Examples of two grouping alternatives are illustrated in figure 12 for both upper and lower wing covers. Grouping 2 (fig. 12(b)) is more restrictive than grouping 1 (fig. 12(a)) as it results in a more uniform (more producible) distribution of angle  $\phi$ . Once a grouping is defined, the optimization is repeated with the grouped variables input as constants in the optimization procedure. The purpose of this operation is to adjust the remaining free variables

to the new situation (new load path, new constraints becoming critical) which is created by altering the previous optimization result by grouping. Such adjustment by means of reoptimization restores a major part of the mass reduction gained by means of the original optimization (ref. 24). The results of the reoptimization are shown in table IV in the form of sandwich cover face-sheet total mass for the two groupings portrayed in figures 12(a) and (b). The table lists a 9.3-percent mass reduction gained by freeing  $\phi$  in addition to thicknesses, when compared with a reference ( $0^\circ$ ,  $\pm 45^\circ$ ,  $90^\circ$ ) design in which only the thicknesses are free. That mass reduction diminishes to 7.8 percent and 6.2 percent for groupings 1 and 2, respectively. The results indicate that two-thirds of the weight reduction realized by freeing the variable  $\phi$  can still be recovered when that variable is grouped and frozen. As expected, a more restrictive grouping corresponds to a lower percentage of recovery.

### Summary of Trends

Results reviewed in the preceding section appear to have design implications which can be summarized as follows.

Structural mass savings of 56 percent can be obtained for the subject airframe sized for strength only by changing from baseline titanium to pure composite construction of a high-strength (low Young's modulus) material. Mass reductions due to hybrid construction and use of composite material having lower strength but higher Young's modulus values are contained in that range. These mass reductions correspond to the use of a conventional  $0^\circ$ ,  $\pm 45^\circ$ ,  $90^\circ$  lay-up and a constant depth for the sandwich wing cover panels.

Further mass reductions on the order of 5 percent are possible if the number of design variables is increased to include orientation angles and sandwich depth. Most of that increased mass reduction potential is realizable if one addresses the producibility constraints by reoptimization with grouping and/or linking. These structural mass trends are depicted in figure 13, which shows (from left to right) the structural mass of the construction variants discussed in the foregoing, relative to the titanium baseline taken as 100 percent.

Except for the thickness design variables, sandwich depth consistently emerges as the variable most effectively influencing structural mass, suggesting a design with stepped or tapered-wing sandwich cover depths. The high Young's modulus material option appears to be the most effective means to counter the stiffness decrease associated with the change to composite materials.

### Convergence and Computational Requirements

The method's convergence is illustrated in figure 14 by iteration histories for the two configurations B and HM/H. Loops I and II (see fig. 1) are typically performed in a ratio varying from 1/1 to 3/1, that is, one to three aerodynamic loads updates (loop I) per one structural resizing (loop II). One complete iteration is defined as one execution of resizing loop described by the flow chart in figure 1 plus the associated load update loop executions. Quantities plotted (fig. 14) are structural mass, wing root bending moment, and wing tip deflection.

The curves indicate a smooth monotonic convergence for both configurations. All three quantities, and particularly the root bending moment, stabilize very fast in the baseline configuration. Convergence is not as fast for the bending moment and tip deflection in the composite construction because of the composite wing's greater flexibility, and consequent stronger coupling between the structural deflections and aerodynamic loads. The mathematical optimization of each panel of the wing cover requires from 8 to 15 objective function and constraint evaluations and terminates mostly by the criterion of small consecutive changes of the objective function. In summary, the whole iterative procedure appears to be well behaved and converges to a reasonable tolerance within five iterations. Approximately, this consumes as much computer resources as seven repetitions of a complete aerodynamic load and finite-element structural analyses of the subject airframe.

The procedure depicted in figure 1 is composed of sequential execution of several computer programs. The major programs are listed in table V with their field lengths and CPU time for one execution for a CONTROL DATA CYBER 175 computer system. Computer performance indicates acceptable consumption of computer resources and generally produces a wing optimization within five iterations, CPU 700<sub>10</sub> sec, and less than 24 hours of turnaround time.

#### CONCLUDING REMARKS

A computerized procedure to generate cross-sectional dimensions and fiber orientations for composite airframe structures has been developed. A methodology of its application to a wing structural synthesis has been established involving the selection of the type of construction, material, and design variables. The algorithm unifies computations of aeroelastic loads, stresses, and deflections and optimal structural sizing and fiber orientations in an open-ended system of integrated computer programs. Aerodynamic loads analysis, finite-element structural analysis, and a mathematical-optimization technique are the main components of the procedure. Each wing cover panel is optimized separately for minimum mass subject to stress, strain, local buckling, and minimum gage constraints. The design variables are ply thicknesses and fiber orientation angles. Experience gained in application to a low-aspect-ratio wing of a large supersonic transport airframe leads to the following conclusions regarding the procedure:

1. A unified iterative method combining structural resizing and aeroelastic load computation converges smoothly and monotonically for both metal and composite wings.
2. Use of mathematical programming in an integrated open-ended and modular system of computer programs provides flexibility needed for variety of design variables, types of material and construction, and constraints; including some of the producibility requirements that have to be dealt with in composite structures. However, since individual panels are optimized separately, the resulting design is expected to be near, but not at, the minimum total mass design.
3. Computer performance of the method as implemented on the CONTROL DATA CYBER 175 computer indicates acceptable consumption of computer resources and

generally produces a wing optimization within five iterations, CPU 700<sub>10</sub> sec, and less than 24 hours of turnaround time.

In the particular application, structural mass reductions in excess of 50 percent result when changing from baseline titanium to pure composite construction. Only about one-third of that mass saving is realized when the change is made to a hybrid construction which retains the titanium network of ribs and spars.

Varying the sandwich panel depth, in addition to the layer thicknesses, is found to be a significantly more effective means of reducing the structural mass than varying the ply orientation angles. Generally, the mass reduction is associated with loss of stiffness. That loss can be reduced by use of a higher Young's modulus material.

Langley Research Center  
National Aeronautics and Space Administration  
Hampton, VA 23665  
January 5, 1979

## REFERENCES

1. Sobieszczanski, Jaroslaw; McCullers, L. Arnold; Ricketts, Rodney H.; Santoro, Nick J.; Beskenis, Sharon D.; and Kurtze, William L.: Structural Design Studies of a Supersonic Cruise Arrow Wing Configuration. Proceedings of the SCAR Conference - Part 2, NASA CP-001, [1977], pp. 659-683.
2. Turner, M. J.; and Hoy, J. M.: Titanium and Advanced Composite Structures for a Supersonic Cruise Arrow Wing Configuration. Proceedings of the SCAR Conference - Part 2, NASA CP-001, [1977], pp. 579-602.
3. Sakata, I. F.; and Davis, G. W.: Advanced Structures Technology Applied to a Supersonic Cruise Arrow-Wing Configuration. Proceedings of the SCAR Conference - Part 2, NASA CP-001, [1977], pp. 603-636.
4. McCullers, L. A.: Automated Design of Advanced Composite Structures. Structural Optimization Symposium, L. A. Schmit, Jr., ed., AMD - Vol. 7, American Soc. Mech. Eng., Nov. 1974, pp. 119-133.
5. Stroud, W. Jefferson; Agranoff, Nancy; and Anderson, Melvin S.: Minimum-Mass Design of Filamentary Composite Panels Under Combined Loads: Design Procedure Based on a Rigorous Buckling Analysis. NASA TN D-8417, 1977.
6. Agarwal, Banarsi; and Davis, Randall C.: Minimum-Weight Designs for Hat-Stiffened Composite Panels Under Uniaxial Compression. NASA TN D-7779, 1974.
7. Williams, Jerry G.; and Mikulas, Martin M., Jr.: Analytical and Experimental Study of Structurally Efficient Composite Hat-Stiffened Panels Loaded in Axial Compression. NASA TM X-72813, 1976. (Also available as AIAA Paper No. 75-754.)
8. Haftka, Raphael T.; and Starnes, James H., Jr.: Applications of a Quadratic Extended Interior Penalty Function for Structural Optimization. AIAA J., vol. 14, no. 6, June 1976, pp. 718-724.
9. Haftka, Raphael T.: Automated Procedure for Design of Wing Structures To Satisfy Strength and Flutter Requirements. NASA TN D-7264, 1973.
10. Stroud, W. Jefferson; Dexter, Cornelia B.; and Stein, Manuel: Automated Preliminary Design of Simplified Wing Structures To Satisfy Strength and Flutter Requirements. NASA TN D-6534, 1971.
11. McCullers, L. A.; and Naberhaus, J. D.: Automated Structural Design and Analysis of Advanced Composite Wing Models. Comput. & Struct., vol. 3, no. 4, July 1973, pp. 925-935.
12. Khot, N. S.: Computer Program (OPTCOMP) for Optimization of Composite Structures for Minimum Weight Design. AFFDL-TR-76-149, U.S. Air Force, Feb. 1977.

13. Schmit, L. A., Jr.; and Farshi, B.: Some Approximation Concepts for Structural Synthesis. AIAA J., vol. 12, no. 5, May 1974, pp. 692-699.
14. Giles, Gary L.; and McCullers, L. A.: Simultaneous Calculation of Aircraft Design Loads and Structural Member Sizes. AIAA Paper No. 75-965, Aug. 1975.
15. Sobieszczanski, Jaroslaw: Building a Computer-Aided Design Capability Using a Standard Time Share Operating System. Integrated Design and Analysis of Aerospace Structures, R. F. Hartung, ed., American Soc. Mech. Eng., c.1975, pp. 93-112.
16. Giles, Gary L.: Computer-Aided Methods for Analysis and Synthesis of Supersonic Cruise Aircraft Structures. Proceedings of the SCAR Conference - Part 2, NASA CP-001, [1977], pp. 637-657.
17. Sobieszczanski, Jaroslaw: Sizing of Complex Structure by the Integration of Several Different Optimal Design Algorithms. Paper presented at the AGARD Lecture Series No. 70 on Structural Optimization (Hampton, Virginia), Oct. 1974.
18. Ashton, J. E.; Halpin, J. C.; and Petit, P. H.: Primer on Composite Materials: Analysis. Technomic Pub. Co., Inc., c.1969.
19. Jones, Robert M.: Mechanics of Composite Materials. McGraw-Hill Book Co., c.1975.
20. Lekhnitskii, S. G. (S. W. Tsai and T. Cheron, transl.): Anisotropic Plates. Gordon & Breach Sci. Publ., Inc., c.1968.
21. Viswanathan, A. V.; Tamekuni, M.; and Baker, L. L.: Buckling Analysis for Anisotropic Laminated Plates Under Combined Inplane Loads. IAF Paper 74-038, Sept.-Oct. 1974.
22. Zoutendijk, G.: Methods of Feasible Directions. Elsevier Pub. Co., 1960.
23. Vanderplaats, Garret N.: The Computer for Design and Optimization. Computing in Applied Mechanics, R. F. Hartung, ed., AMD - Vol. 18, American Soc. Mech. Eng., c.1976, pp. 25-48.
24. Taig, I. C.; and Kerr, R. I.: Optimisation in Construction of the Jaguar and Other Military Aircraft. Aircraft Eng., vol. 45, Jan. 1973, pp. 9-11.

TABLE I.- MATERIAL PROPERTIES

[Room temperature, 20° C (68° F)]

Young's modulus, E		Poisson's ratio, $\nu$	Ultimate tensile strength, $F_{tu}$		Ultimate compressive strength, $F_{cu}$		Stress allowable for cruise, $F_{ac}$		Mass density of ply material, $\rho$		Fiber orientation
GN/m <sup>2</sup>	ksi		MN/m <sup>2</sup>	ksi	MN/m <sup>2</sup>	ksi	MN/m <sup>2</sup>	ksi	kg/m <sup>3</sup>	lb/in <sup>3</sup>	
Titanium alloy <sup>a</sup>											
110	$16 \times 10^3$	0.3	827	120	868	126	155	22.5	4429	0.16	
Low Young's modulus graphite-polyimide <sup>b</sup>											
138	$20 \times 10^3$	0.31	2033	295	1998	290	351	51	1550	0.056	Parallel
7.8	$1.13 \times 10^3$	.18	115	16.7	113	16.4			1550	.056	Perpendicular
High Young's modulus graphite-polyimide <sup>b</sup>											
276	$40 \times 10^3$	0.29	1020	148	868	126	176	25.6	1605	0.058	Parallel
12.4	$1.8 \times 10^3$	.013	46	6.7	39.3	5.7			1605	.058	Perpendicular

<sup>a</sup>Minimum gage per face sheet, 0.04 cm (0.015 in.).

<sup>b</sup>Properties anticipated for 1986; fiber volume assumed to be 60 percent.

Mass of honeycomb core, kg/m<sup>3</sup> (lb/in<sup>3</sup>) . . . . . 89 (0.0032)  
 Mass per unit area for adhesive bonding face sheets to core, kg/m<sup>2</sup> (lb/ft<sup>2</sup>) . . . . . 0.036 (0.288)  
 Conservative strain allowable for applied load . . . . . 0.004  
 Single ply thickness, cm (in.) . . . . . 0.0102 (0.004)



TABLE II.- MASS<sup>a</sup> AND STIFFNESS DATA FOR SEVERAL CONFIGURATIONS

Configuration (b)	Mass, kg (lbm)					Tip deflection, m (in.)	Fundamental frequency, Hz
	Rib and spar caps	Rib and spar webs	Core	Covers	Total		
B	7 814 (17 228)	4416 (9736)	4 755 (10 482)	10 285 (22 675)	27 270 (60 120)	6.5 (256)	1.182
LM/H	7 814 (17 228)	4399 (9698)	4 980 (10 978)	4 636 (10 221)	21 829 (48 125)	8.0 (313)	.897
HM/H	7 814 (17 228)	4347 (9584)	4 915 (10 836)	6 558 (14 457)	23 634 (52 105)	3.9 (155)	1.099
LM/P	0	1733 (3821)	4 954 (10 922)	5 304 (11 694)	11 992 (26 437)	10.4 (409)	1.082
HM/P	0	1400 (3087)	4 879 (10 756)	7 531 (16 602)	13 810 (30 445)	3.9 (153)	1.076
LM/H-CA	7 814 (17 228)	4382 (9661)	4 917 (10 840)	6 292 (13 872)	23 406 (51 601)	6.3 (247)	1.033

<sup>a</sup>Including nonoptimum mass.

<sup>b</sup>Hybrid and pure composite configurations are for fixed core depth and ply orientations of 0°, ±45°, and 90°.

TABLE III.- FREE DESIGN VARIABLES FOR LM/H CONFIGURATION<sup>a</sup>

Free design variables	Mass, kg (lbm)					Wing tip deflection, m (in.)	Fundamental frequency, Hz
	Caps 1	Webs 2	Core 3	Covers 4	Total 5		
$t_0, t_{\pm 45}, t_{90}$	7 814 (17 228)	4399 (9698)	4 980 (10 978)	4 636 (10 221)	21 829 (48 125)	8.0 (313)	0.897
$t_0, t_{\pm 45}, t_{90}, \gamma$	7 814 (17 228)	4410 (9722)	4 983 (10 986)	4 541 (10 011)	21 748 (47 947)	8.1 (319)	.896
$t_0, t_{\pm \phi}, t_{90}, \phi$	7 814 (17 228)	4358 (9608)	4 993 (11 008)	4 288 (9 453)	21 453 (47 297)	8.3 (327)	.866
$t_0, t_{\pm \phi}, t_{90}, \gamma, \phi$	7 814 (17 228)	4374 (9644)	5 000 (11 024)	4 085 (9 006)	21 274 (46 902)	8.4 (329)	.861
$t_0, t_{\pm 45}, t_{90}, t_c$	7 814 (17 228)	4418 (9739)	3 920 (8 642)	4 212 (9 285)	20 363 (44 894)	8.0 (314)	.897
$t_0, t_{\pm 45}, t_{90}, t_c, \gamma$	7 814 (17 228)	4435 (9778)	3 947 (8 702)	4 095 (9 027)	20 291 (44 735)	8.0 (316)	.898
$t_0, t_{\pm \phi}, t_{90}, t_c, \phi$	7 814 (17 228)	4410 (9722)	3 898 (8 594)	3 831 (8 445)	19 908 (43 889)	8.6 (338)	.847
$t_0, t_{\pm \phi}, t_{90}, \phi, \gamma$	7 814 (17 228)	4382 (9661)	3 980 (8 774)	3 607 (7 953)	19 784 (43 616)	8.6 (339)	.845

<sup>a</sup>All masses include nonoptimum mass.

TABLE IV.- RESULTS OF GROUPING DESIGN VARIABLE  $\phi$  FOR  
LM/H CONFIGURATION

Panel grouping	Cover mass	
	kg	lbm
No grouping, $\phi$ free	1396	3077
No grouping, $\phi$ fixed at 45°	1539	3393
Grouping 1 (fig. 12(a))	1419	3129
Grouping 2 (fig. 12(b))	1443	3181

TABLE V.- COMPUTER RESOURCES

Program	Field length	CPU time, sec (a)
SPAR - a finite element analysis program	165 100	73.7
Jig-shape computation	40 100	1.3
Woodward-Carmichael aerodynamics	52 100	30
Generation of pressure coefficients for camber and twist	52 100	.3
Airplane-balance calculation	52 100	.8
Rib and spar web resizing	50 100	.9
Skin resizing	120 100	93.9

<sup>a</sup>CONTROL DATA CYBER 175 computer system.

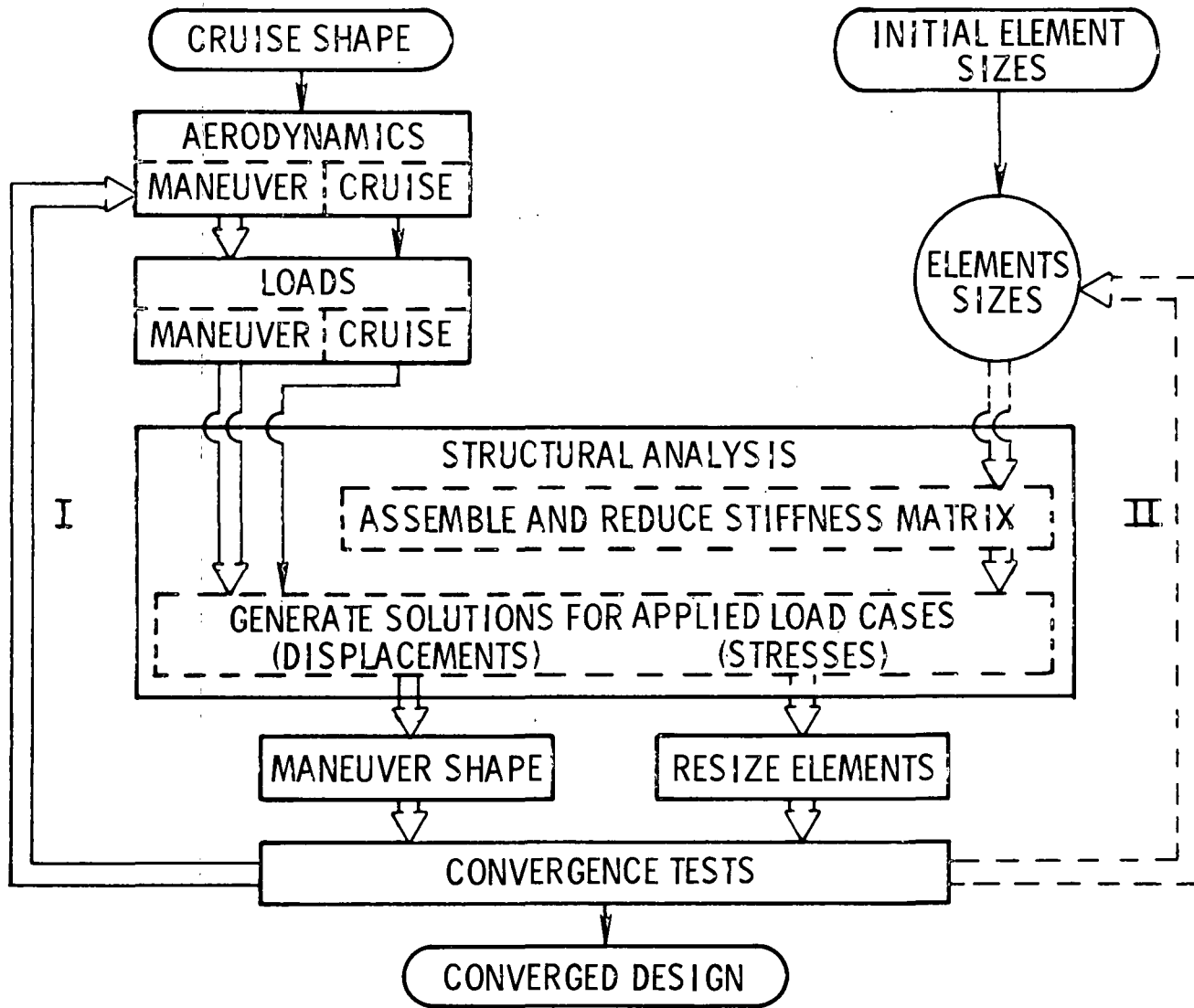


Figure 1.- Iterative procedures for aeroelastic loads computation (loop I) and wing cover resizing (loop II) (from ref. 14).

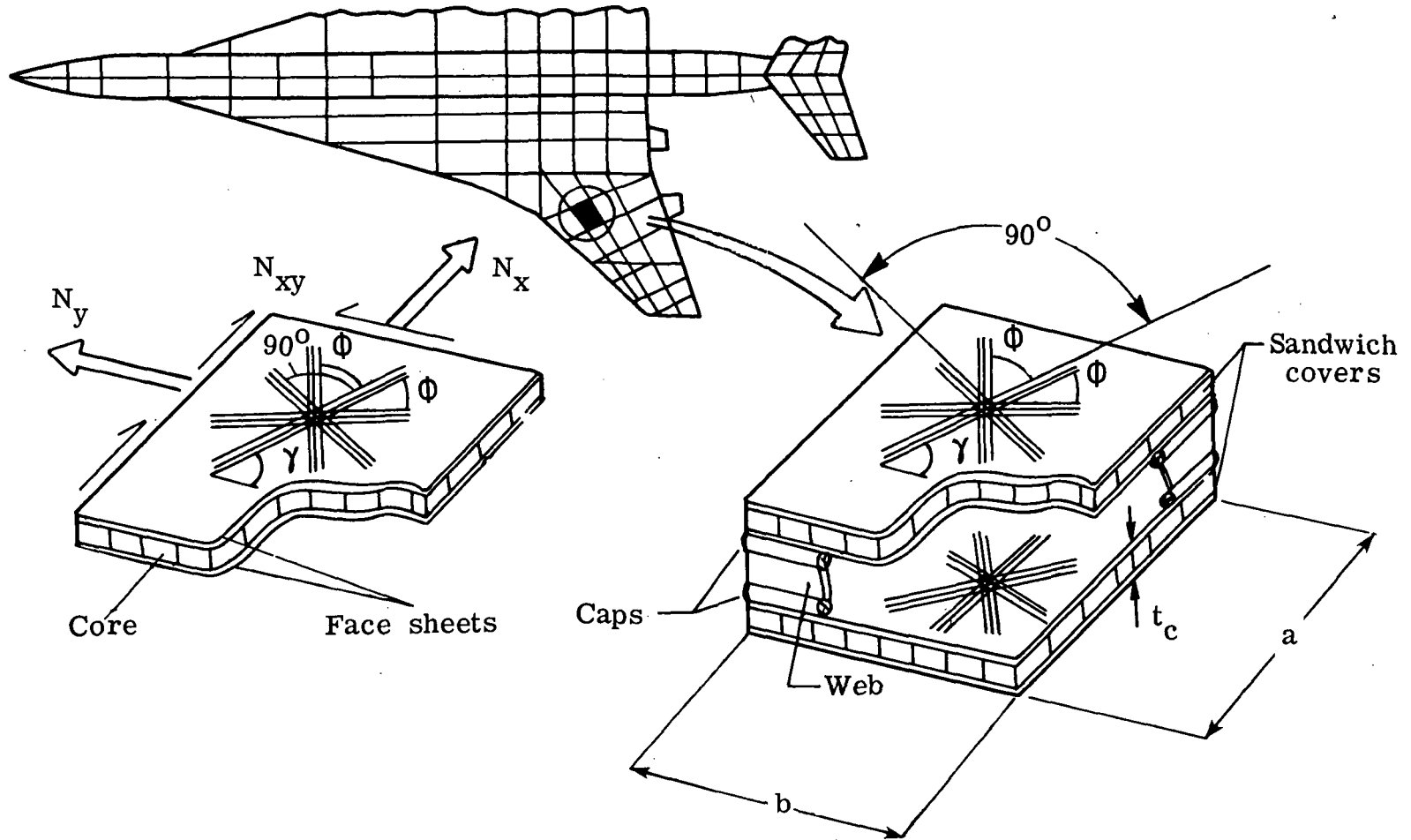


Figure 2.- Composite sandwich panel and design variables.

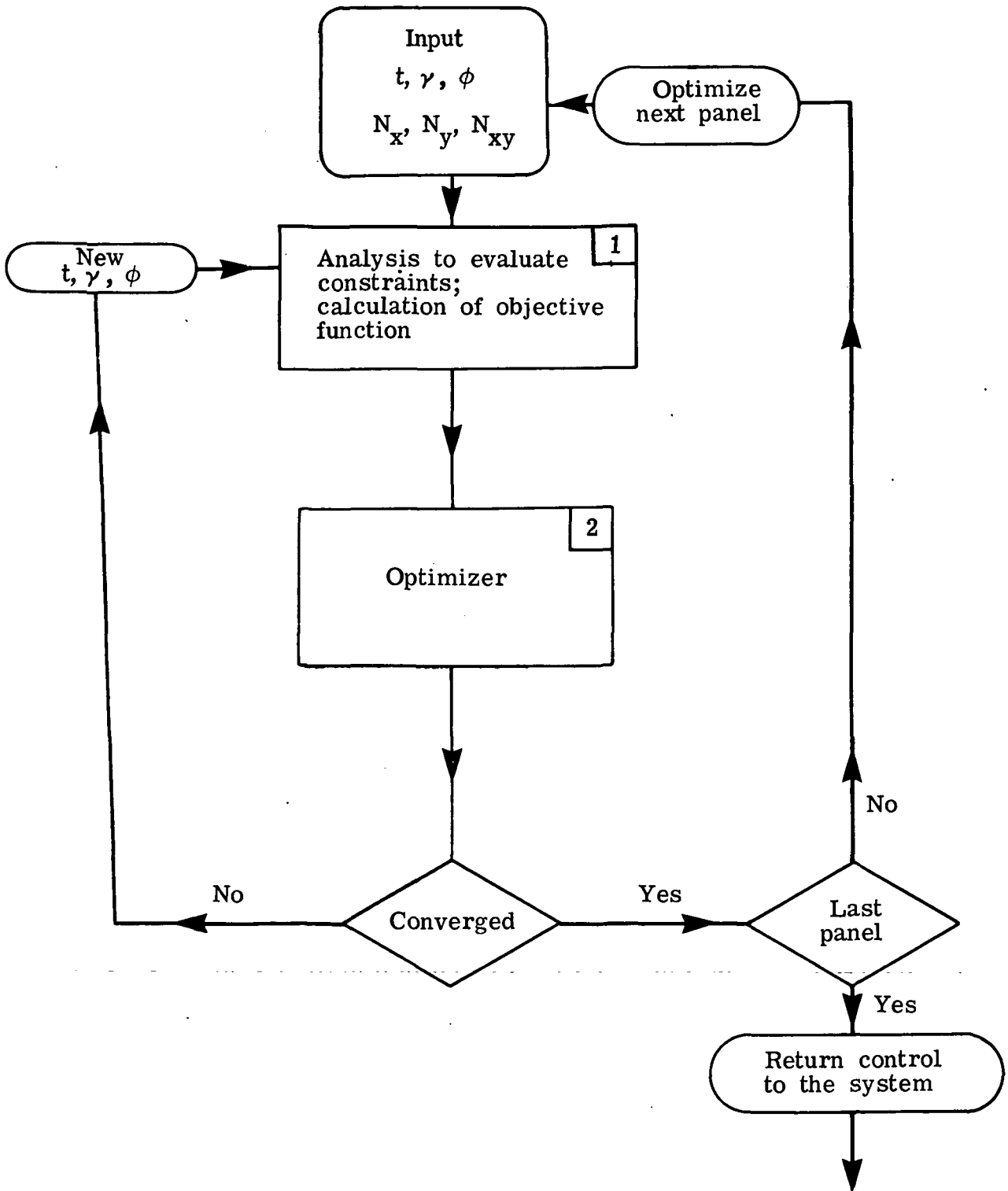


Figure 3.- Resizing-procedure flow chart.

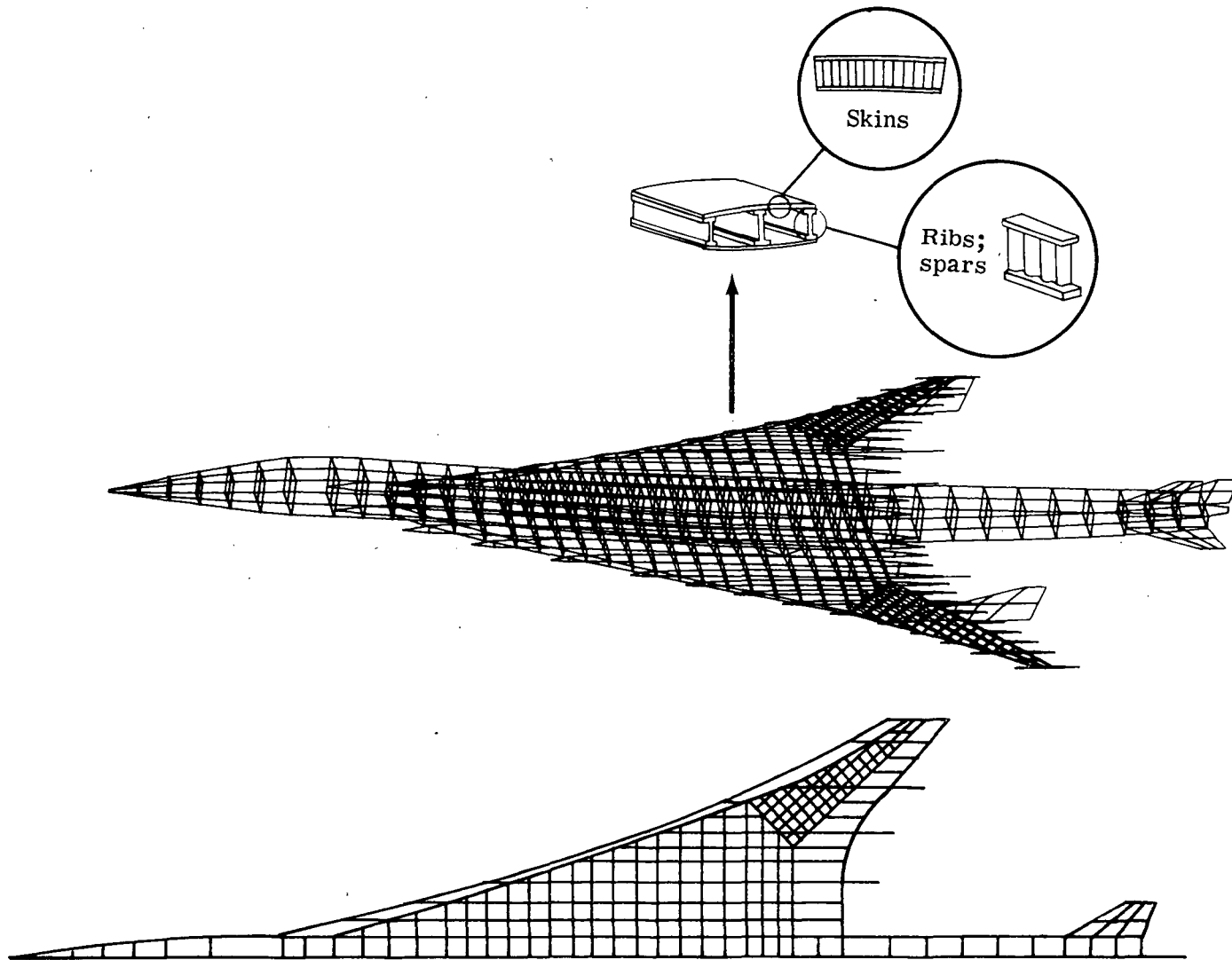
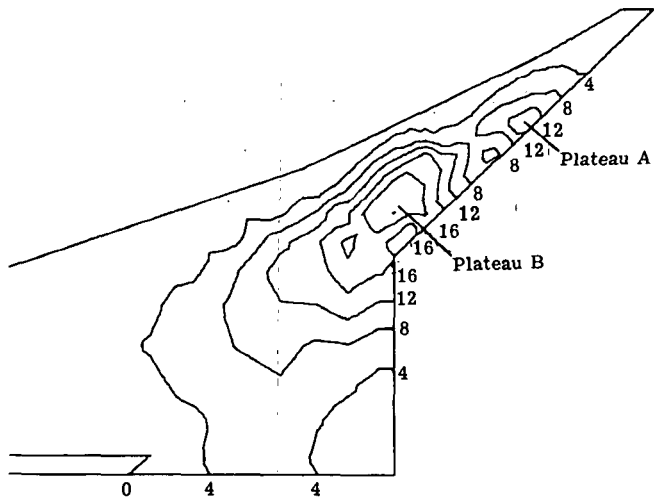
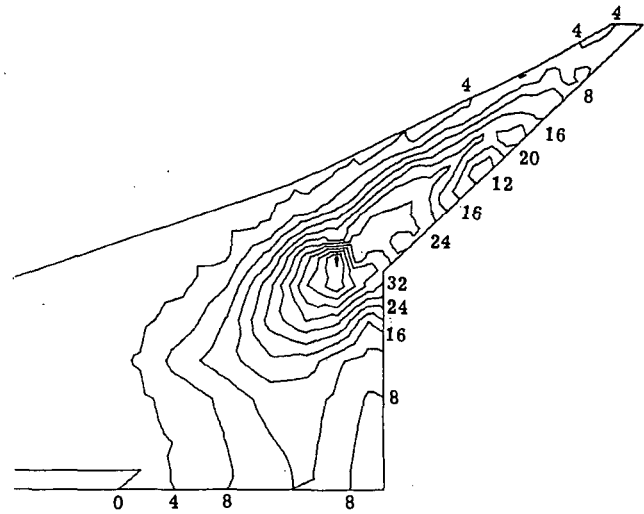


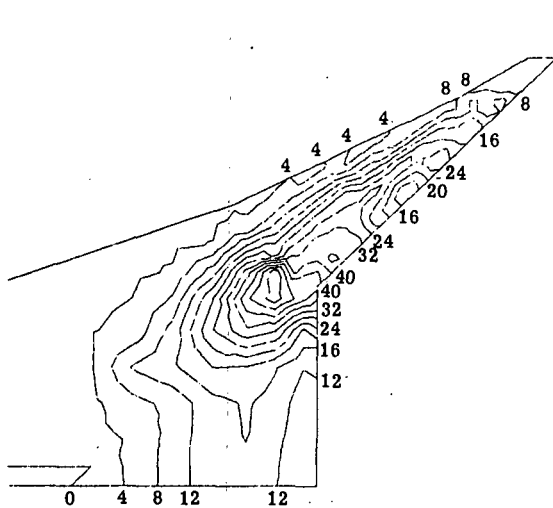
Figure 4.- Two projections of finite-element model. Inset shows construction details.



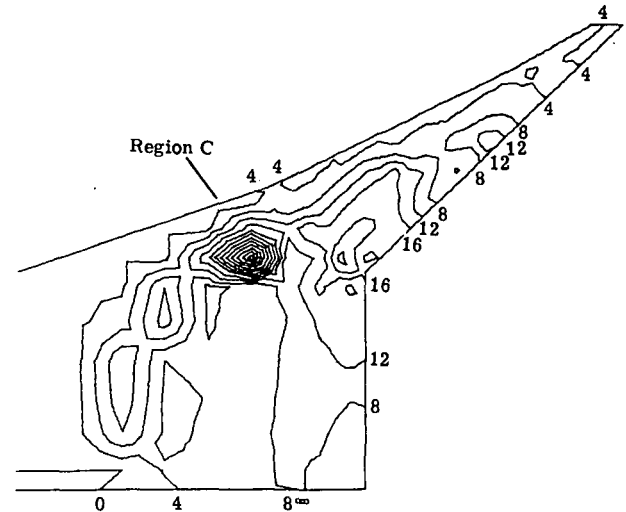
(a) Baseline configuration.



(b) HM/H configuration.



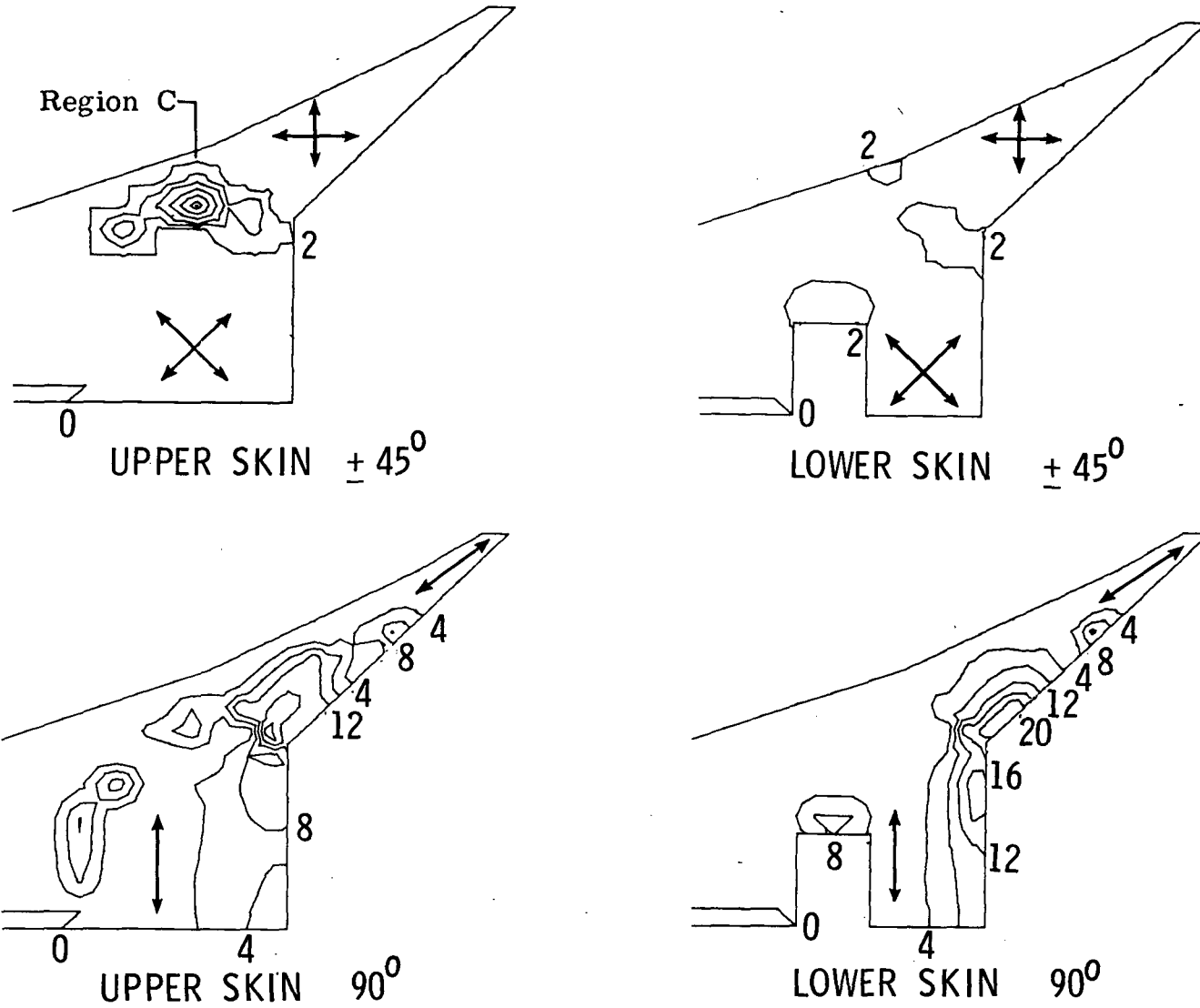
(c) HM/P configuration.





(d) LM/H configuration.

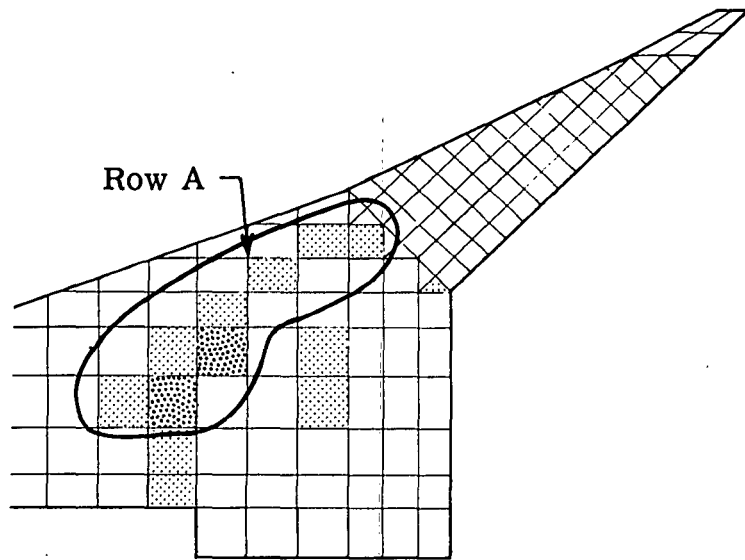
Figure 5.- Skin thickness contours in 0.0254 cm (0.01 in.).



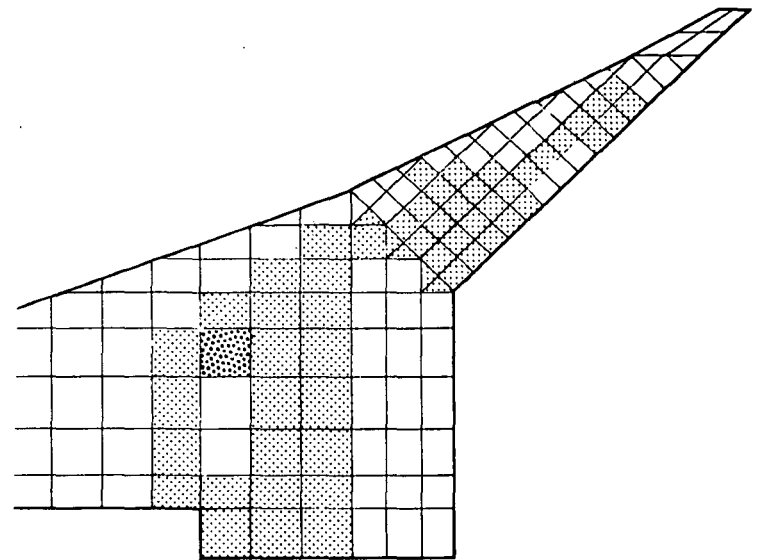


(e)  $90^\circ$  and  $\pm 45^\circ$  orientation angles for LM/H configuration. (Arrows indicate fiber orientations.)

-  Buckling critical for low Young's modulus
-  Buckling critical for high and low Young's modulus



(a) LM/H configuration.



(b) LM/P configuration.

Figure 6.- Buckling critical panels for two configurations.

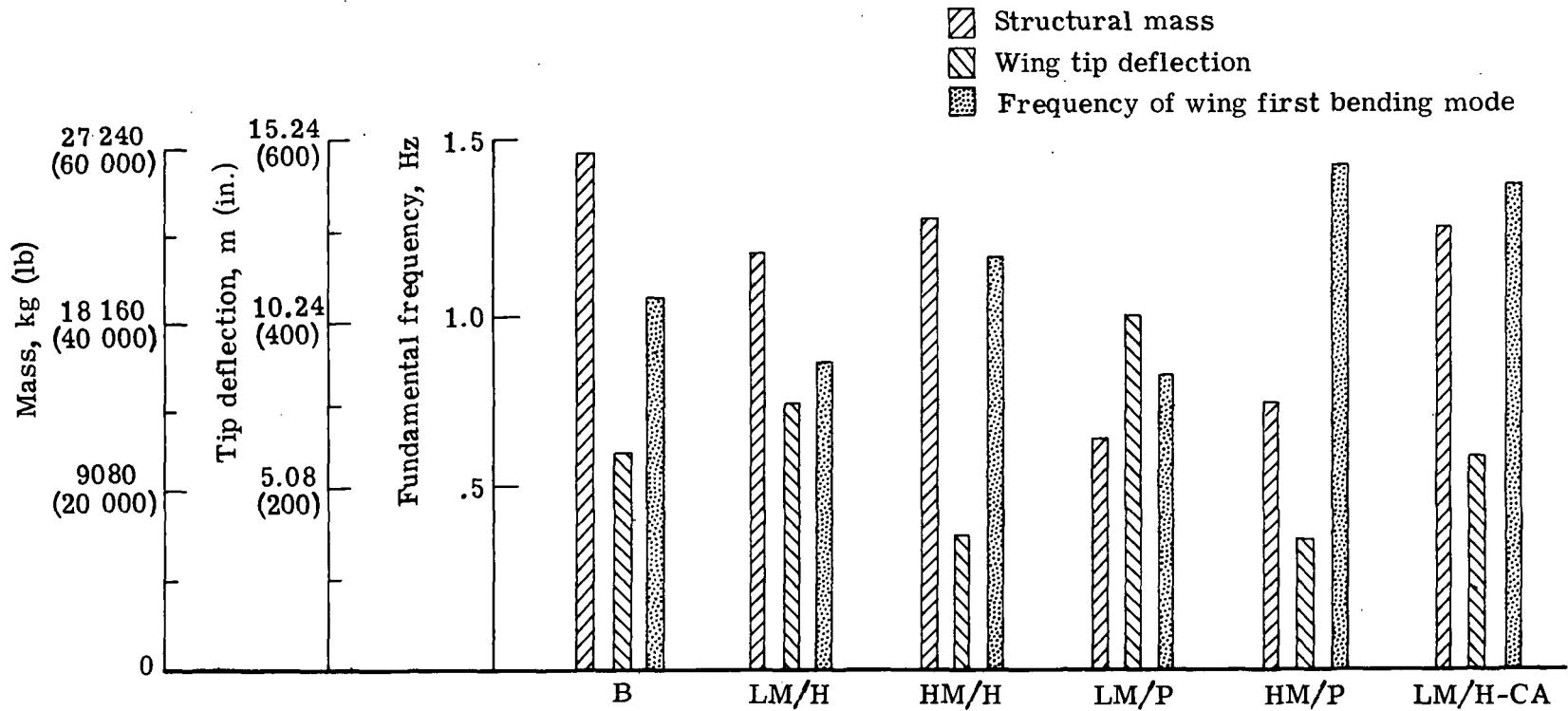
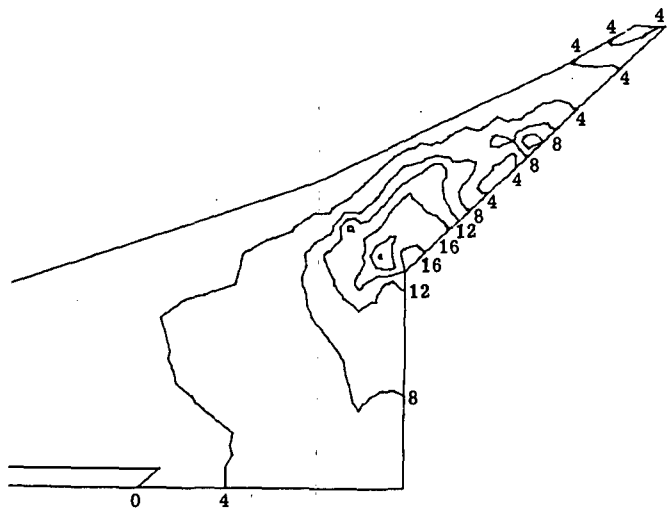
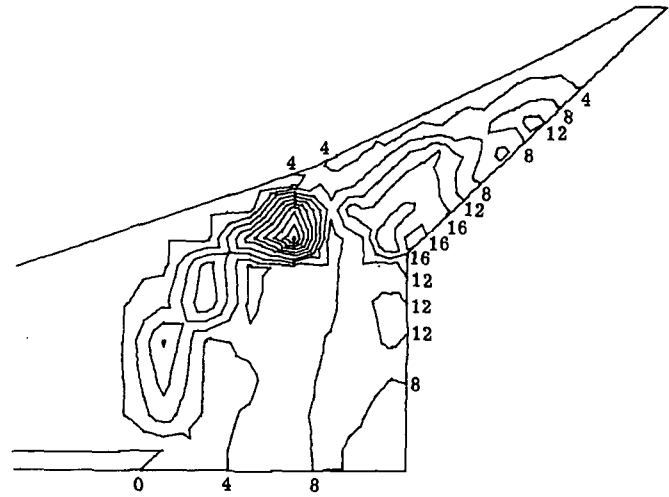


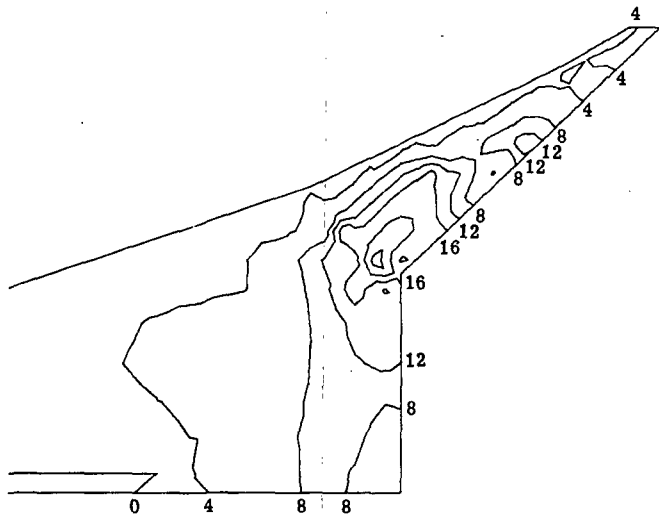
Figure 7.- Mass, tip deflection, and fundamental frequency for wing configurations.



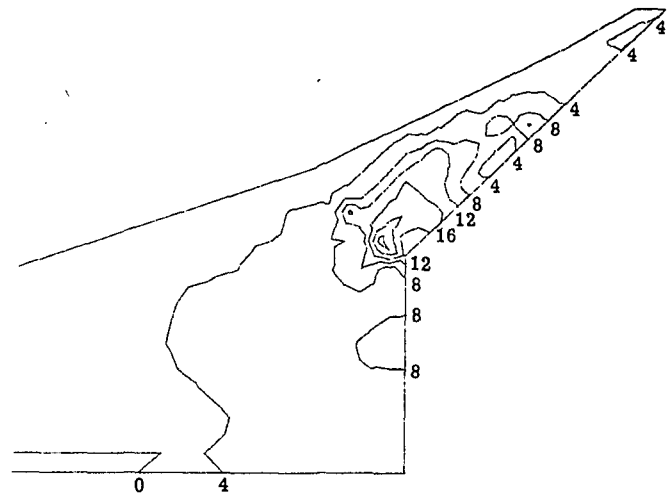
(a)  $t$ ,  $t_c$ , and  $\phi$ .



(b)  $t$  and  $\gamma$ .



(c)  $t$  and  $t_c$ .



(d)  $t$ ,  $t_c$ ,  $\phi$ , and  $\gamma$ .

Figure 8.- Skin thickness contours in 0.0254 cm (0.01 in.) for different combinations of design variables for LM/H configuration.





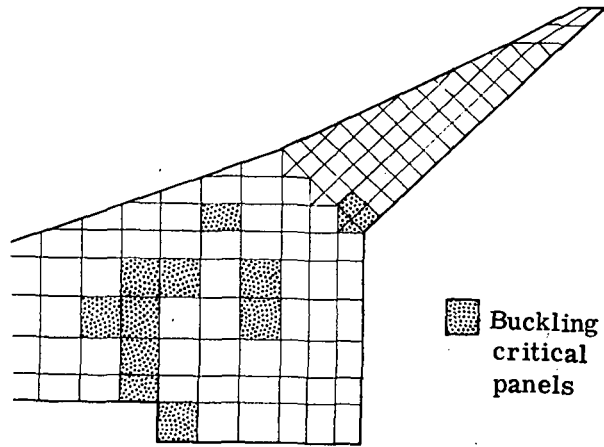
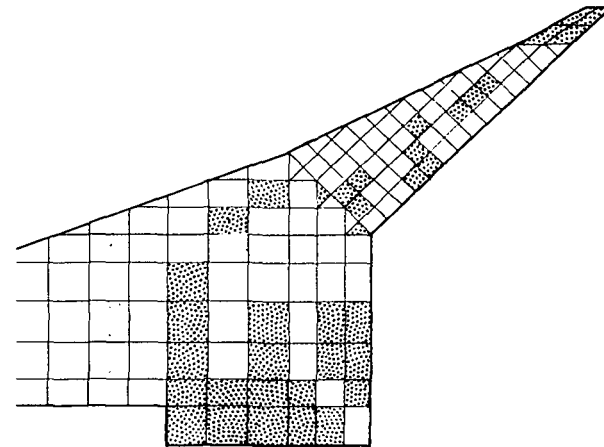
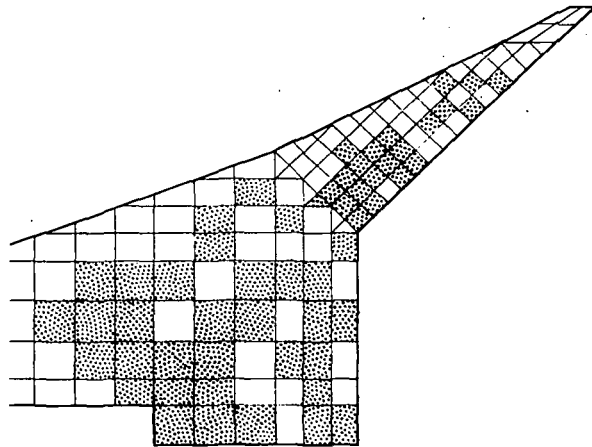
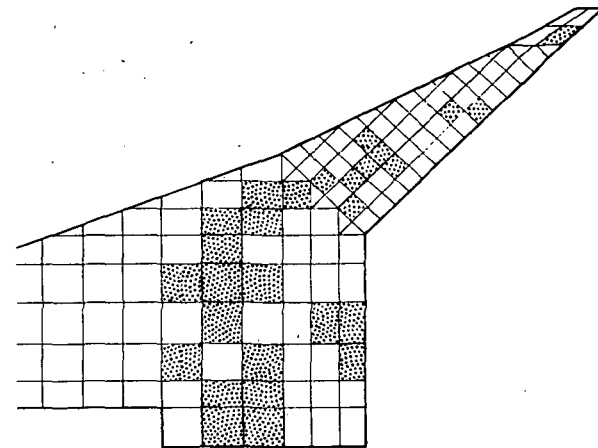
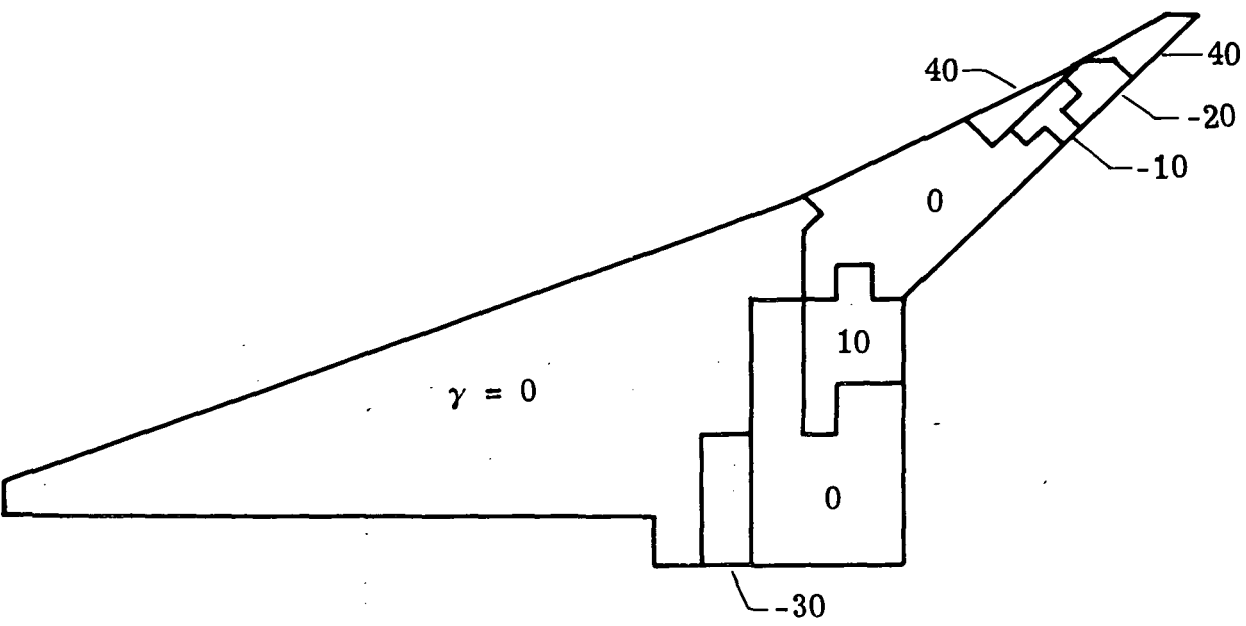
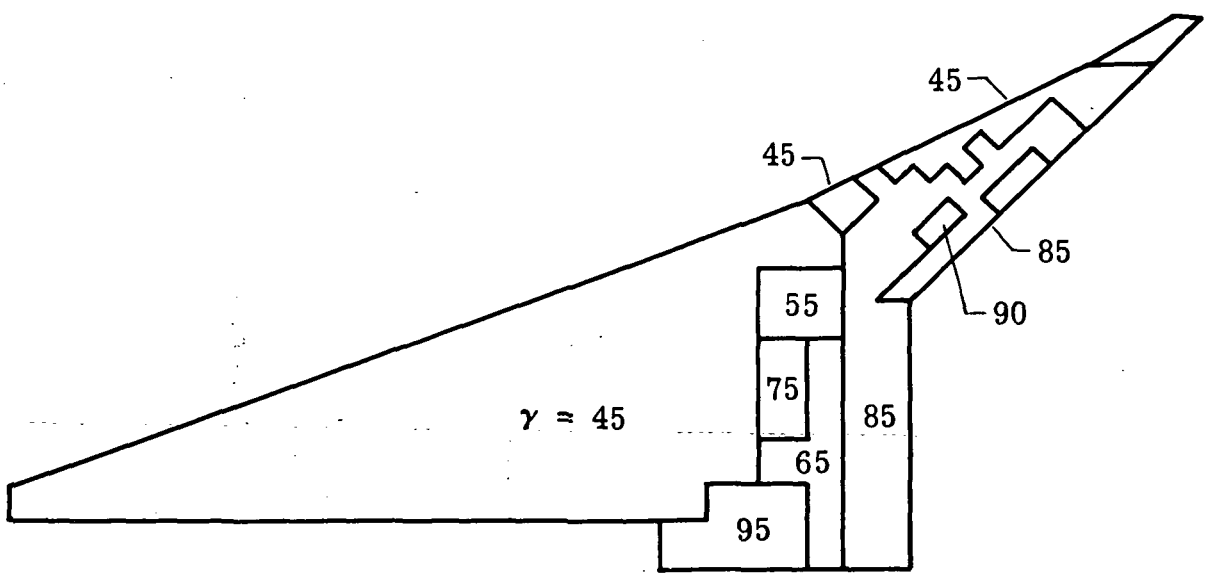
(a)  $t$  and  $\gamma$ .(b)  $t$ ,  $t_c$ , and  $\phi$ .(c)  $t$  and  $t_c$ .(d)  $t$ ,  $t_c$ ,  $\gamma$ , and  $\phi$ .

Figure 10.- Buckling critical panels for different combinations of design variables for LM/H configurations.



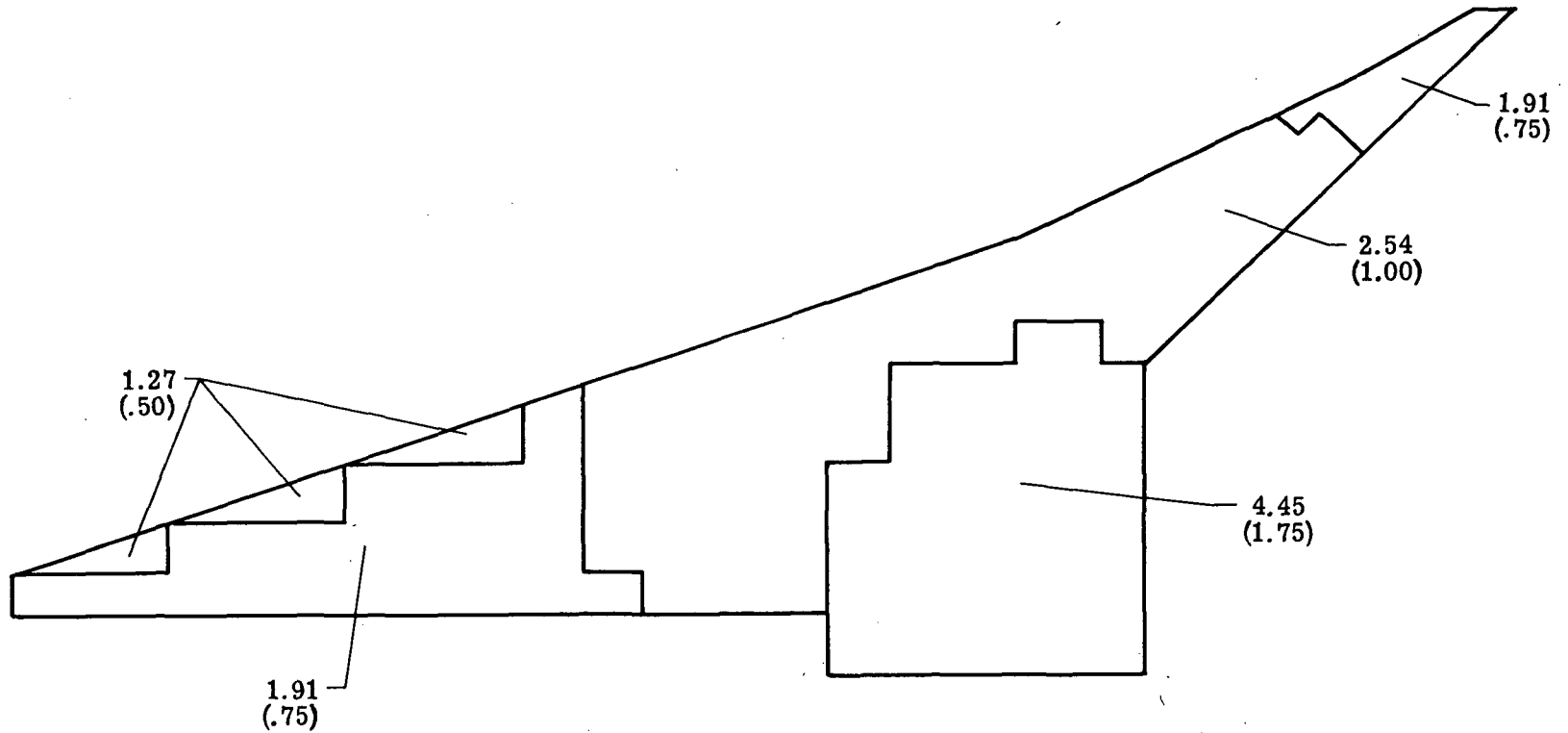
(a) Orientation angle  $\gamma$ . (Values are given in degrees.)



(b) Orientation angle  $\phi$ . (Values are given in degrees.)

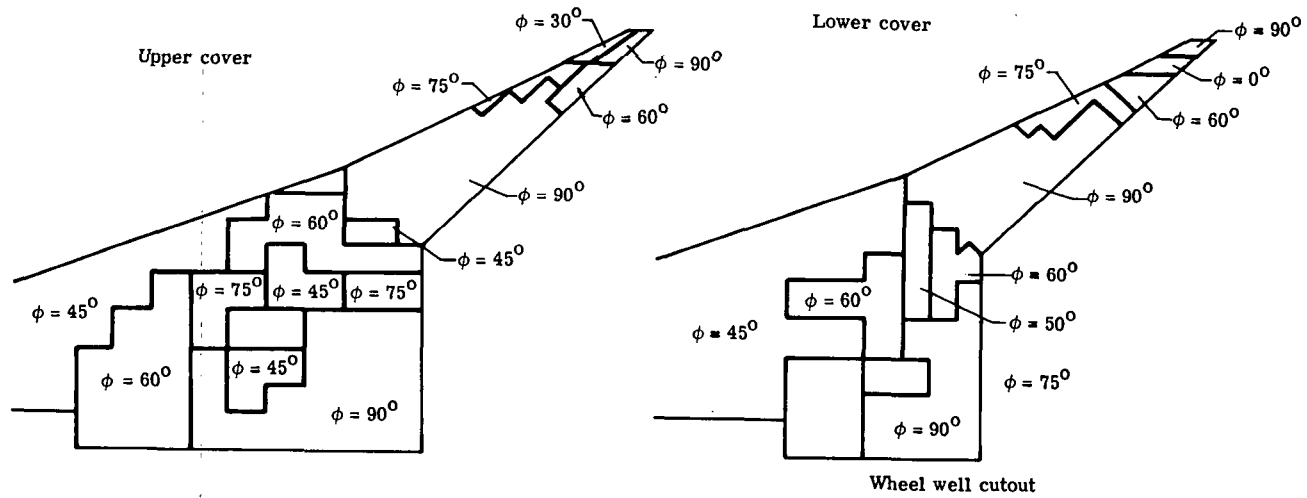
Figure 11.- Grouping of panels for design variables  $\gamma$ ,  $\phi$ , and  $t_c$ .



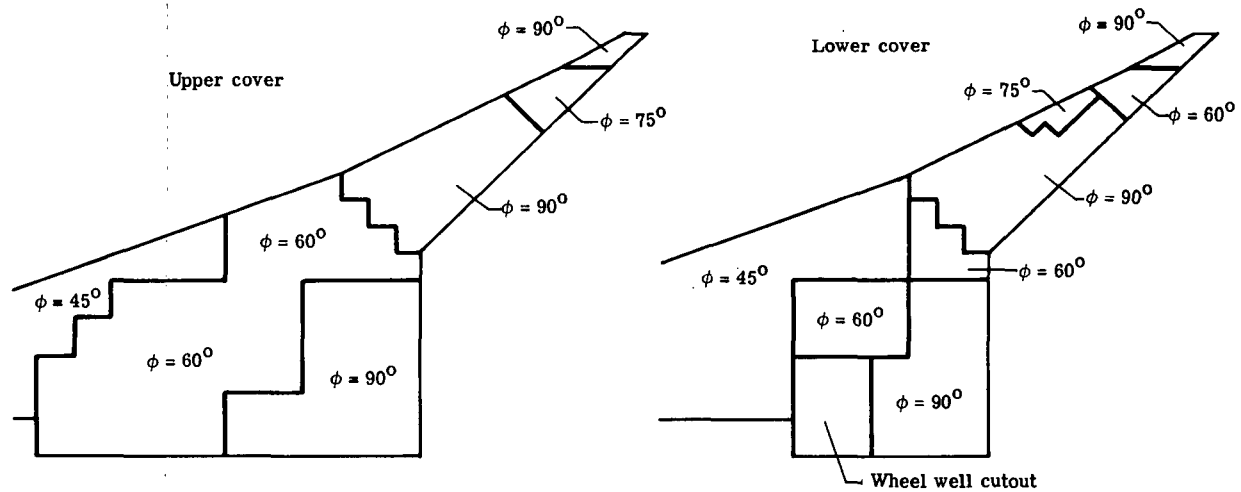


(c) Constant core depth  $t_c$ . (Values are given in cm (in.).)

Figure 11.- Concluded.



(a) Grouping 1.



(b) Grouping 2.

Figure 12.- Grouping of design variable  $\phi$  for upper and lower wing covers.

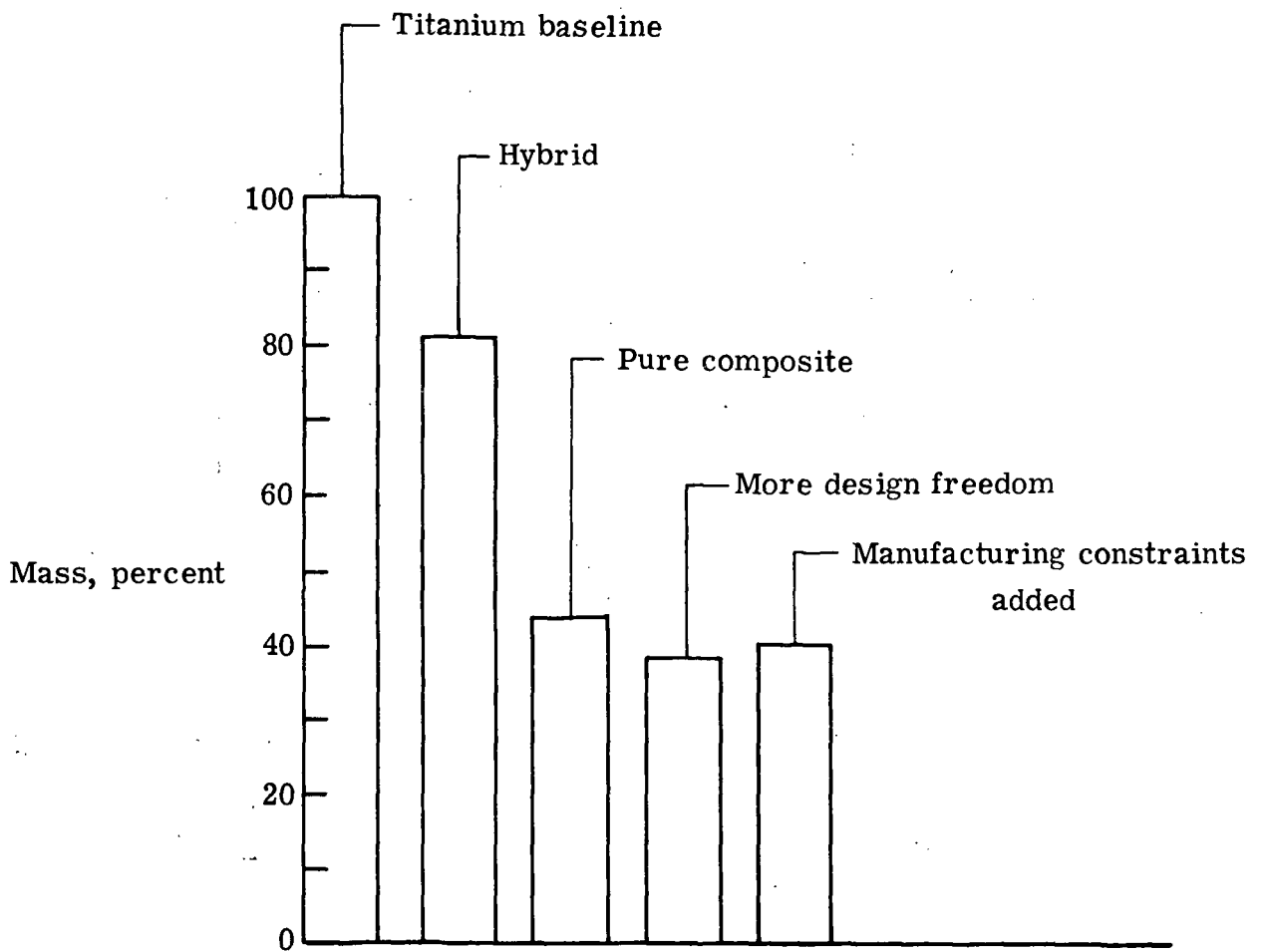


Figure 13.- Effects on structural mass of changes in construction material, design variables, and constraints.

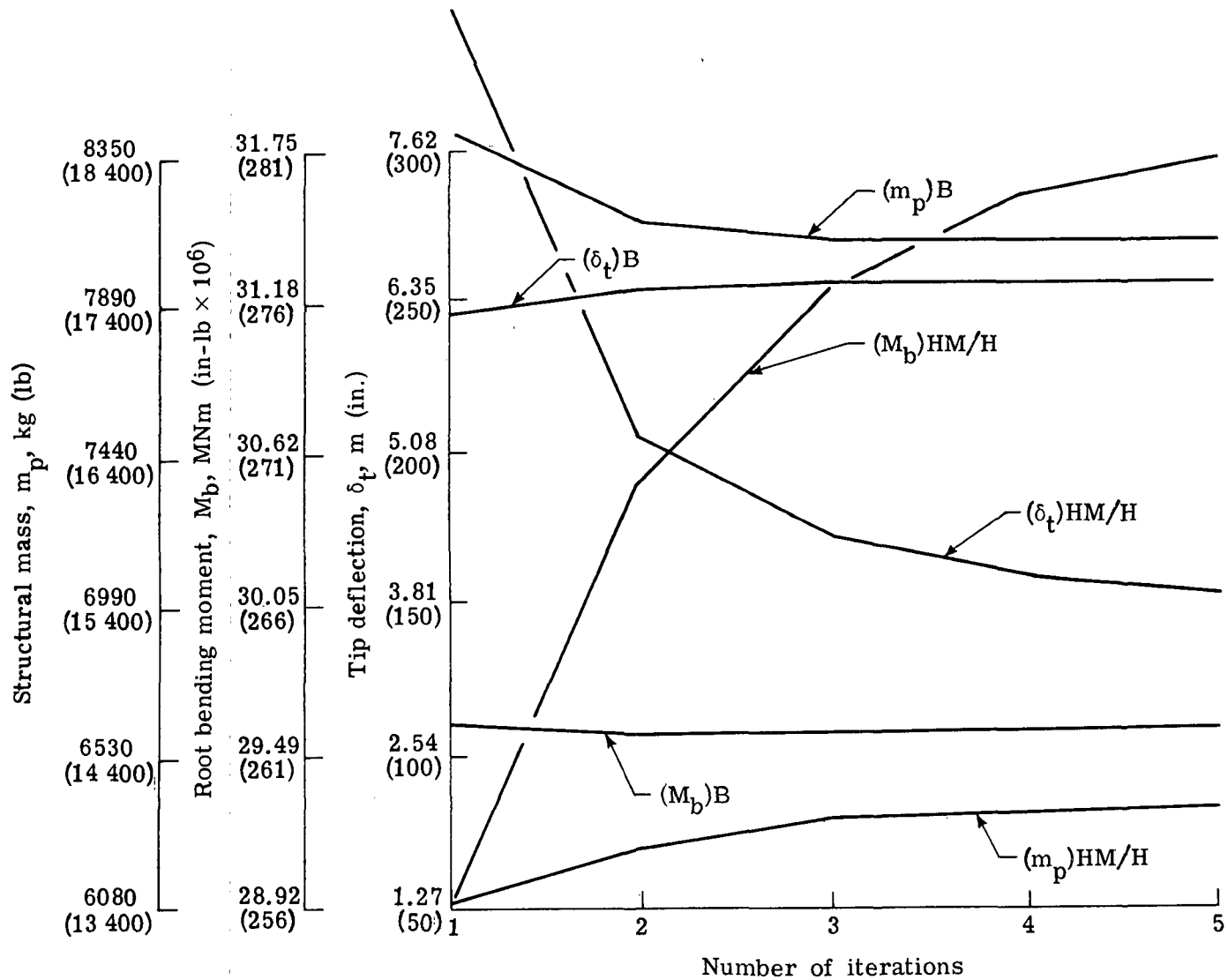


Figure 14.- Iteration histories for B configuration and HM/H configuration.

1. Report No. NASA TP-1300	2. Government Accession No.	3. Recipient's Catalog No.	
4. Title and Subtitle AN INTEGRATED COMPUTER PROCEDURE FOR SIZING COMPOSITE AIRFRAME STRUCTURES		5. Report Date February 1979	6. Performing Organization Code
		8. Performing Organization Report No. L-11817	10. Work Unit No. 743-01-01-02
7. Author(s) Jaroslaw Sobieszczanski-Sobieski		11. Contract or Grant No.	
9. Performing Organization Name and Address NASA Langley Research Center Hampton, VA 23665		13. Type of Report and Period Covered Technical Paper	
		14. Sponsoring Agency Code	
12. Sponsoring Agency Name and Address National Aeronautics and Space Administration Washington, DC 20546		15. Supplementary Notes	
16. Abstract  A computerized algorithm to generate cross-sectional dimensions and fiber orientations for composite airframe structures is described, and its application in a wing structural synthesis is established. The algorithm unifies computations of aeroelastic loads, stresses, and deflections, as well as optimal structural sizing and fiber orientations in an open-ended system of integrated computer programs. A finite-element analysis and a mathematical-optimization technique are the main components of the procedure.			
17. Key Words (Suggested by Author(s)) Structural optimization Composite materials Supersonic airframes		18. Distribution Statement Unclassified - Unlimited  Subject Category 61	
19. Security Classif. (of this report) Unclassified	20. Security Classif. (of this page) Unclassified	21. No. of Pages 43	22. Price* \$4.50

National Aeronautics and  
Space Administration

THIRD-CLASS BULK RATE

Postage and Fees Paid  
National Aeronautics and  
Space Administration  
NASA-451



Washington, D.C.  
20546

Official Business  
Penalty for Private Use, \$300

**NASA**

POSTMASTER: If Undeliverable (Section 158  
Postal Manual) Do Not Return

---